Available online at www.sciencedirect.com
SCIENCE DIRECT®
Journal of Sound and Vibration 274 (2004) 953–984
JOURNAL OF SOUND AND VIBRATION
www.elsevier.com/locate/jsvi

A study on the dynamic stability of a cylindrical shell conveying a pulsatile flow of hot fluid

N. Ganesan*, Ravikiran Kadoli

Machine Dynamics Laboratory, Indian Institute of Technology Madras, Chennai 600 036, India

Received 21 January 2003; accepted 5 June 2003

Abstract

The flow of hot fluid having a harmonic component superposed on the mean flow velocity is considered flowing through an insulated cylindrical shell. The cylindrical shell will be subjected to thermal load due to the flow of hot fluid. The semi-analytical finite element forms the basis for modelling the structural continuum under the influence of temperature and the flowing fluid. The fluid flowing through the cylindrical shell is incompressible and linear potential flow theory is used to formulate the fluid domain. Bernoulli's principle and impermeability conditions of the fluid are the basis for a coupled fluid–structure interaction analysis. Model reduction technique in conjunction with the fourth order Runge–Kutta method using Gill's coefficient is adopted to compute the state transition matrix which provides the stability information of the periodic system. The results of the theoretical studies are presented related to instability regions due to a pulsatile flow of hot fluid through a cylindrical shell. Hot fluid at various magnitude of constant temperature limited by the critical thermal buckling temperature is considered in the study. The effect of fluid temperature and excitation parameter on the behavior of dynamic instability of the system is examined.

1. Introduction

Pumps like the reciprocating type and gear pumps used to discharge fluid into the circulatory system, in general, will have flow velocity variations about the mean flow. Hot fluid circulation is typically encountered in hot water heating system and distribution, steam generating stations, petroleum industries, nuclear power stations and the likes. The piping and other accessories in the circuit are generally well insulated to prevent heat loss. Pulsating flow of fluid especially in heat

*Corresponding author. Tel.: +91-44-2351365; fax: +91-44-2350509.
E-mail address: nganesan@iitm.ac.in (N. Ganesan).

0022-460X/$ - see front matter © 2003 Elsevier Ltd. All rights reserved.
doi:10.1016/S0022-460X(03)00658-8

transfer process and equipments has considerable significance from the point view of heat transfer rates. Generally the problems related to flow-induced vibrations are encountered in the power generation industry and processing industries; in spite these being complex there has been enormous contribution by many researchers in understanding and providing solutions. Looking in this direction recently, Weaver et al. [1] have reviewed various problems like (i) turbulence-induced vibrations in parallel flow occurring over surfaces of structures and cross-flow over beams and tubes, (ii) mechanism of vorticity shedding and its associated excitation problems, (iii) fluidelastic instability, (iv) axial flow-induced vibrations and instabilities and (v) the effect of two phase flow regimes on vibration parameters. The mechanism associated with these problems and the mathematical models to analyze the same have been addressed.

Research activities in the area of dynamics of pipes conveying fluid, parametric and combination resonances in piping system due to pulsating flow and the findings thereof has been considered to be of valuable information to the industrial sections. One of the earliest articles containing reviews related to the research work in the area of dynamics and dynamic stability of pipes conveying fluid was published by Paidoussis and Issid [2]. Paidoussis and Issid derived the equation of motion for a flexible pipe conveying fluid which is more general in many respects like, effects of external pressurization and external tension were included, the derivation takes into account the longitudinal acceleration of the fluid, hence can be applied to studies when flow contains harmonic components. They used Kelvin–Voigt type model for the pipe material in order to account for internal dissipation. Thorough investigations on dynamics of pipe conveying fluid with simply supported ends, clamped–clamped ends and cantilevered pipes were presented. They considered the effect of viscoelastic damping on the stability of the system. The difference in the behavior of the system with low and high mass ratio was also presented. Apart form this, studies related to pipes containing harmonically varying flow can also be found. Parametric instability boundaries were computed based on the Bolotin's method. Various configurations of the pipes like pinned–pinned, clamped–clamped and cantilevered were considered in the study. The effect of with and without viscous damping and viscoelastic damping on parametric instability boundaries were compared. The effect of flow velocity and viscous damping on the principal regions of instability were also studied. Paidoussis and Sundararajan [3] carried out theoretical investigations on the parametric and combination resonances in continuous flexible pipe conveying a pulsating flow. The boundaries of the regions of parametric resonance were obtained by Bolotin's method and boundaries of the combination resonance were computed using the Numerical Floquet analysis. It was found that in the case of a pipe with clamped ends combination resonances are associated with the sum of the eigenfrequencies, while for cantilevered pipes they are associated with the difference of the eigenfrequencies. Subsequent to this work, Paidoussis and Issid [4] carried out experimental investigations on clamped–clamped and cantilevered pipes conveying harmonically disturbed fluid in order to observe parametric resonances and combination resonances and compared the experimental results with theoretical results. They used silicon rubber pipes, water at low velocity was considered. Pioneering studies related to dynamic instability of pipes conveying fluctuating fluid were from Chen [5] followed by Ginsberg [6] and Paidoussis and Issid [2]. Ginsberg [6] derived the general equations of motion for small transverse displacement of a pipe conveying fluid based on the transverse force exerted by the flowing fluid. For the case of a simply supported pipe Galerkin method was utilized to obtain the solution. The dynamic instability regions were evaluated and it was shown that the region of

dynamic instability increases with increased amplitude of fluctuation. Ariaratnam and Namachchivaya [7] carried out dynamic stability studies on cylindrical pipes for boundary conditions like pinned–pinned and clamped–clamped. Method of averaging was employed to obtain stability boundaries. For large harmonic perturbation they proposed a numerical method based on Floquet theory due to Bolotin to obtain stability boundaries. The effects of flow velocity, dissipative forces, boundary conditions and virtual mass on the extent of the parametric instability regions were discussed. An up-to-date comprehensive survey on the dynamic studies of pipes conveying fluid has been complied by Paidoussis and Li [8]. This review encompasses most of the topics right from the basic study on simple flexible pipes with usual boundary conditions to the present day understanding of the problem in terms of non-linear analysis and chaotic dynamics. Paidoussis [9] has again looked into topics on flow-induced instabilities in tubular structures, dynamics and stability of cylindrical structures with external axial flow, flow-induced vibration due to flow of fluid in the annular space of a coaxial cylindrical shells, instabilities caused by cross-flow of fluid over a bundle and/or array of tubes as found in heat exchanger, high pressure steam generators, and reported a brief review on these topics. Bohn and Herrmann [10] had carried out studies on the dynamic behavior of articulated pipes (two straight rigid pipe segment being suspended) conveying fluid with small periodic disturbances. They illustrated the importance of the magnitude of low rate oscillation on the occurrence of parametric and combination resonances. They further obtained an algebraic criterion for minimum flow rate amplitude so that one can avoid the parametric resonance. Lee et al. [11] developed a new theory for the dynamics of pipe conveying fluid so as to solve practical problems encountered due to operation of valves and pumps. They used Newton's law of motion to derive the equation to address the vibration of pipeline and used deformable moving control volume concept to derive fluid equations.

Gorman et al. [12] derived the non-linear equation of motion of a flexible pipe conveying unsteady flowing fluid. Their model includes the effect of radial shell vibration of pipes, initial axial tensions within the pipes besides considering the Poisson and friction coupling. The dynamic response of a pipe line conveying fluid with a pulsating flow has been illustrated. Zhang et al. [13] have carried out studies on the vibratory characteristics of initially tensioned orthotropic cylindrical shells conveying fluid. New finite element formulation developed on the basis of three-dimensional theory of elasticity and the Eulerian equations are used. Their analysis is restricted to linear systems even though non-linear strain-displacement is used to derive the geometric stiffness matrix. Further Zhang et al. [14] have considered the initial stresses due to hydrodynamic pressure within the shell and its influence on the vibratory characteristics of a cylindrical shells conveying fluid. Amabili et al. [15] carried out investigation on the non-linear dynamics and stability of circular cylindrical shells containing fluid flow. They used the non-linear Donnell's shallow shell theory to model large amplitude shell motion and linear potential flow theory to describe the fluid–structure interaction. Subsequently Amabili and Garziera [16] extended their studies to shells with flowing fluid as well as immersed in axial flow of fluid. Here they used Flugge theory of shell to describe the shell motion. Now the study encompasses various effects like non-uniform boundary conditions, radial pressure, initial pre-stress etc. Jayaraj et al. [17,18] formulated a semi-analytical finite element for the fluid domain to study the dynamics of shells conveying fluid. They conducted extensive studies on the shells made of isotropic as well as orthotropic materials. They could illustrate the divergence type buckling as the flow velocity reaches a critical velocity. The lowest critical velocity of fluid causing the shell to lose static stability coincides with the mode of

the shell vibration having the lowest natural frequency. Apart from this their analysis could also predict the various characteristics regions involved in the dynamic behavior of shells conveying fluid like the shell becoming unstable when velocity of water attains critical velocity and it remains so in a small region of fluid flow, restabilizing as the flow velocity increases and further as velocity is increased the modes join which lead to coupled mode flutter, these results are well established in the past by Paidoussi and Issid [2]. Compressible as well as incompressible fluid characteristics have been considered in formulating the fluid domain. In the compressible fluid domain the velocity potential satisfies the wave equation (in acoustic sense) and in the case of incompressible fluid the velocity potential satisfies the Laplace equation. Further, Jayaraj et al. [19] carried out studies on the parametric excitation in cylindrical shells conveying pulsating fluid. They considered incompressible fluid to model the fluid flow domain. One is aware of the numerical overflow problems in case of parametrically excited system with large number equations. This problem was circumvented by the model reduction of the coupled fluid–structure system using the undamped eigenvectors. This has the advantage of understanding the instabilities of the individual modes as well as the instabilities considering various modes together, which has been illustrated in their work. They have studied the parametric instability of bending mode only. Kadoli and Ganesan [20] have carried out studies on the dynamics of shells conveying hot fluid through the clamped–clamped cylindrical shells made of HS-Graphite/Epoxy. The study illustrated the buckling (divergence type instability) of the system due to a steady flow of hot water, at constant temperature, for flow velocities near the critical velocity. Various magnitude of water temperature was considered in the study to determine the influence of the magnitude of water temperature on the critical flow velocities. It was also found that the lowest critical velocity of hot water happens to coincide with the buckling mode of the cylindrical shell having the lowest thermal buckling temperature.

2. Problem definition, analysis and computation approach—a discussion

In this paper a problem in a situation is considered where a displacement type of pump discharges hot fluid into a perfectly insulated cylindrical shell which is a major part of the hot fluid distribution circuit, see Fig. 1. The investigation on the dynamic stability of a system comprising of the insulated cylindrical shell conveying pulsating hot fluid is attempted. The pulsating flow of

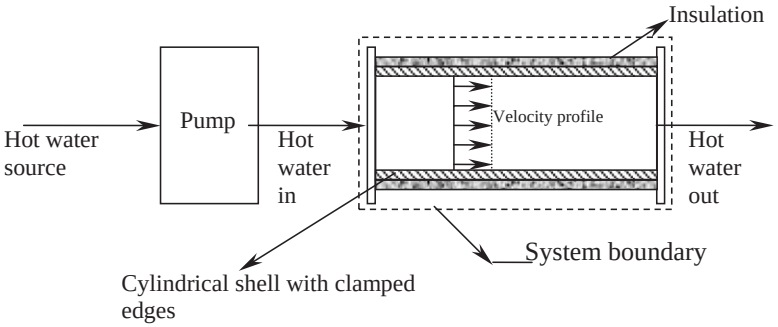

Fig. 1. Schematics of the system under investigation: a cylindrical shell conveying hot fluid.

hot fluid is assumed to have a time-dependent harmonic component superposed on the steady mean flow velocity. The shell is assumed to be perfectly insulated so that heat loss to atmosphere is negligible. This assumption should ensure that under the existing flow conditions the temperature of the shell wall is equal to that of hot fluid.

The inlet and outlet fluid temperature does not vary to a great extent so that uniform temperature is assumed to exist along the length of shell. The presence of hot fluid flowing inside the shell, in effect, is considered to produce thermal loading on the shell. Hence the initial stresses in the shell are accounted for analysis through the geometric stiffness matrix. Water is considered as the working fluid. The flow is assumed to have a uniform velocity profile over internal area of cross-section and the pressure of flowing water is above atmospheric pressure. The hot water has negligible viscosity and it is assumed to be incompressible. Density variation of water at higher temperature is ignored. The cylindrical shell is assumed to have its edges perfectly clamped. Effect of the insulation over the cylindrical shell on the shell dynamics is neglected. There are no studies in the literature related to studies involving parametric excitation of cylindrical shells conveying hot fluid. In the present paper possibly for the first time in literature an attempt is made to study the parametric instability of shell conveying pulsatile hot fluid. Apart from this it is necessary to evaluate the thermal stress influence on the parametric instability.

Ramasamy and Ganesan [21] developed a semi-analytical finite element formulation to study the vibratory characteristics of fluid filled orthotropic cylindrical shells with constrained viscoelastic layer (i.e., viscoelastic layer constrained between the orthotropic lamina). Jayaraj et al. [17–19] used the viscoelastic layer constrained within orthotropic cylindrical shell semi-analytical finite element formulation developed by Ramasamy and Ganesan and coupled with the flowing fluid domain for their studies on the dynamics of shells conveying steady flow of fluid as well as fluctuating fluid. The structural degree of freedom of the viscoelastic layered cylindrical shell is seven (i.e., five-degree-of-freedom for the core and two degree of freedom for the facings). Jayaraj et al. modifies the shell formulation by considering all the three layers made of same material and each layer with equal thickness. It is possible to degenerate the structural equations of the constrained viscoelastic shell so as to carry out analysis for a conventional shell lamina on the lines of first order shear deformation theory, thereby shell lamina will have five-degree-of-freedom viz. $\{u \quad v \quad w \quad \psi_s \quad \psi_\theta\}$. In order to achieve this it is possible to make the thickness of the facings either very small or set to zero and the core layer thickness equal to shell thickness.

Keeping these points in mind and for overall computational work we use the computer code developed by Jayaraj et al. [19] which helps to analyze the parametric instabilities in shells conveying fluid. As stated previously the program is modified so that the additional rotational degrees of freedom of the facings are suppressed and also setting the thickness of the inner and outer facing equal to zero so that it simulates the computation of shell stiffness and mass matrix based on FSDT. In addition to this, the geometric stiffness matrix which is time independent is included in the analysis. This stems from the fact that the shell wall is subjected to thermal loading due to axisymmetric temperature distribution. The fluid domain is for an incompressible fluid. The stability analysis of parametrically excited system generally involves the computation of the transition matrix. The Floquet–Liapunov theorem when used to determine the stability of periodic system involves the determination of the state transition matrix over one period. Friedmann et al. [22] have developed improved numerical integration scheme for obtaining the transition matrix $\Phi_A(T_p, 0)$ in a single integration pass, since $\Phi_A(T_p, 0)$ is independent of the initial

condition. This integration scheme is based on the fourth order Runge–Kutta scheme with Gill's coefficient. Following the work of Friedmann et al., Jayaraj et al. [19] have developed a computer code to compute the transition matrix over one period and hence the eigenvalues of this matrix to obtain the stability information of periodic system. The model reduction technique and the computational procedure to determine the instability/stability regions developed by Jayaraj et al are used in the present work. The current study to start with requires the knowledge of the critical thermal buckling temperature as well as critical velocities of the hot water under steady flow conditions through the shell.

3. Semi-analytical finite element formulation

Semi-analytical finite element for general shells of revolution based on first order shear deformation theory is used to describe the shell vibration behavior. The fluid domain is analyzed using the linear potential theory and the fluid–structure interaction coupling is implement using Bernoulli's principle for unsteady flow and the impermeability condition. Temperature effects due to flow of hot fluid are considered in the analysis and accounted by computing the initial stresses (in case of shell analysis strictly these are stress resultants and moment resultants). Thus we frame a set of equations as a result of uncoupled thermomechanical and coupled fluid–structure interaction approach. The equation describing the system due to pulsating flow of hot fluid will have matrices which are time dependent (or periodic in nature). The solution to the periodic equation involves the computation of the monodromy matrix (or transition matrix). The integration of the state transition matrix is carried out using the fourth order Runge–Kutta method with Gill's coefficient, which gives an indication whether the system is stable or unstable. Even though much the formulation is available in the literature it is outlined here for the sake of completeness.

3.1. Structural domian

The (s, θ, z) co-ordinate system used to describe the mid-surface geometry of the general shells of revolution is illustrated in the Fig. 2. The strain displacement relations for a general shell of revolution are used and hence on appropriate simplification these will be applicable for the analysis of cylindrical shells, conical shells, spherical shells etc. The mid-surface displacements according to the first order shear deformation theory are expressed as

$$u(s, \theta, z, t) = u_o(s, \theta, t) + z\psi_s(s, \theta, t), \tag{1a}$$

$$v(s, \theta, z, t) = v_o(s, \theta, t) + z\psi_\theta(s, \theta, t), \tag{1b}$$

$$w(s, \theta, z, t) = w_o(s, \theta, t), \tag{1c}$$

where u_o, v_o, and w_o are displacement of mid-surface along the s, θ and z direction and ψ_s and ψ_θ are rotations of the normal to the mid-surface along s and θ axes respectively.

$$\mathbf{u}^{\mathrm{T}} = \{ u \quad v \quad w \}. \tag{2}$$

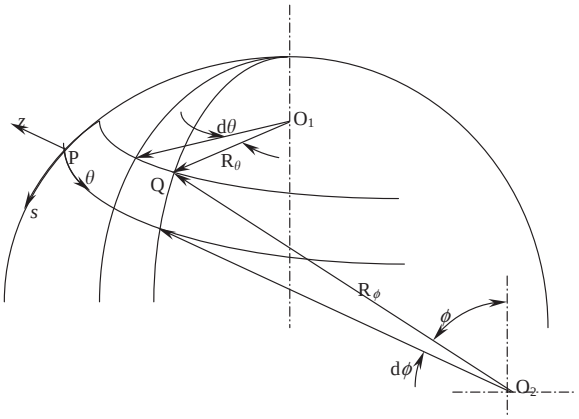

Fig. 2. Description of the co-ordinate system for general shells of revolution.

In the semi-analytical method the generalized displacement field is assumed to depend in the circumferential direction hence these quantities can be expanded by a Fourier series in the θ direction as follows:

$$\begin{Bmatrix} u_o(s,\theta,t) \\ v_o(s,\theta,t) \\ w_o(s,\theta,t) \\ \psi_s(s,\theta,t) \\ \psi_\theta(s,\theta,t) \end{Bmatrix} = \sum_{m=0}^{\infty} \begin{bmatrix} \cos m\theta & 0 & 0 & 0 & 0 \\ 0 & \sin m\theta & 0 & 0 & 0 \\ 0 & 0 & \cos m\theta & 0 & 0 \\ 0 & 0 & 0 & \cos m\theta & 0 \\ 0 & 0 & 0 & 0 & \sin m\theta \end{bmatrix} \begin{Bmatrix} u_{om}(s,t) \\ v_{om}(s,t) \\ w_{om}(s,t) \\ \psi_{sm}(s,t) \\ \psi_{\theta m}(s,t) \end{Bmatrix} \tag{3}$$

'm' indicates the harmonic number (or circumferential mode number).

3.1.1. Stiffness matrix

The semi-analytical finite element formulation for general shells of revolution is based on the first order shear deformation theory. The structural stiffness matrix is derived from the strain energy, Ramalingeswara Rao and Ganesan [23]. The total strain energy in the shell continuum is given by

$$U = U_1 + U_2,$$

where U_1 is the strain energy due to vibratory stresses and U_2 is the strain energy contribution from the initial stresses due to steady state axisymmetric temperature. Strain energy U_1 is given by

$$U_1 = \frac{1}{2}\int_V \{\varepsilon_{ss}\sigma_{ss} + \varepsilon_{\theta\theta}\sigma_{\theta\theta} + \gamma_{\theta z}\tau_{\theta z} + \gamma_{sz}\tau_{sz} + \gamma_{s\theta}\tau_{s\theta}\}\,\mathrm{d}V. \tag{4}$$

The kinematic relations for a doubly curved shells of revolution in the (s,θ,z) co-ordinate based on FSDT are as follows:

$$\varepsilon_{ss} = \frac{1}{A_1}(\varepsilon^o_{ss} + z\kappa^1_s), \quad \gamma_{\theta z} = \frac{1}{A_2}\gamma^o_{\theta z},$$

$$\varepsilon_{\theta\theta} = \frac{1}{A_2}(\varepsilon^o_{\theta\theta} + z\kappa^1_\theta), \quad \gamma_{sz} = \frac{1}{A_1}\gamma^o_{sz},$$

$$\gamma_{s\theta} = \frac{1}{A_1}\frac{1}{A_2}(\gamma^o_{s\theta} + z\kappa^1_{s\theta}),$$

where

$$\frac{1}{A_1} = \frac{1}{(1 + z/R_\phi)}$$

and

$$\frac{1}{A_2} = \frac{1}{(1 + z/R_\theta)}$$

in the above equations R_ϕ and R_θ are the principle radii of curvature of the shell and z is the thickness measured along the z-axis. In the above equation, $\varepsilon_{ss}, \varepsilon_{\theta\theta}, \gamma_{\theta z}, \gamma_{sz}, \gamma_{s\theta}$ are the total strains which comprise of the normal strains and the shear strains: $\varepsilon^o_{ss}, \varepsilon^o_{\theta\theta}, \gamma^o_{\theta z}, \gamma^o_{sz}, \gamma^o_{s\theta}$ referred to mid-surface and $\kappa^1_s, \kappa^1_\theta, \kappa^1_{s\theta}$, the change in curvature of the mid-surface normal. For a general shell of revolution these strain components are given below:

$$\varepsilon^o_{ss} = \frac{\partial u_o}{\partial s} + \frac{w}{R_\phi}, \quad \varepsilon^o_{\theta\theta} = \frac{1}{r}\frac{\partial v_o}{\partial \theta} + \frac{u_o}{r}\cos\phi + \frac{w_o}{r}\sin\phi,$$

$$\gamma^o_{\theta z} = \phi_\theta - \frac{v_o}{r}\sin\phi + \frac{1}{r}\frac{\partial w_o}{\partial \theta},$$
$$\gamma^o_{s\theta} = \frac{1}{r}\frac{\partial u_o}{\partial \theta} + \frac{\partial v_o}{\partial s} - \frac{v_o}{r}\cos\phi,$$
$$\gamma^o_{sz} = \phi_s - \frac{u_o}{R_\phi} + \frac{\partial w_o}{\partial s},$$

$$\kappa^1_s = \frac{\partial \phi_s}{\partial s}, \quad \kappa^1_\theta = \frac{1}{r}\frac{\partial \phi_\theta}{\partial \theta} + \frac{\phi_s}{r}\cos\phi,$$

$$\kappa^1_{s\theta} = \frac{1}{r}\frac{\partial \phi_s}{\partial \theta} + \frac{\partial \phi_\theta}{\partial s} - \frac{\phi_\theta}{r}\cos\phi + \frac{\sin\phi}{r}\frac{\partial v_o}{\partial s} + \frac{1}{R_\phi r}\frac{\partial u_o}{\partial \theta} - \frac{v_o}{R_\phi r}\cos\phi.$$

Accordingly it follows that the strain vector will comprise of

$$\boldsymbol{\varepsilon}^{\mathrm{T}} = \{\varepsilon^o_{ss}\varepsilon^o_{\theta\theta}\gamma^o_{s\theta}\kappa^1_s\kappa^1_\theta\kappa^1_{s\theta}\gamma^o_{sz}\gamma^o_{\theta z}\} \text{ or } \boldsymbol{\varepsilon} = \begin{Bmatrix} \boldsymbol{\varepsilon}^0 \\ \boldsymbol{\kappa}^1 \\ \boldsymbol{\gamma}^0 \end{Bmatrix},$$

where $(\boldsymbol{\varepsilon}^0)^{\mathrm{T}} = \{\varepsilon^o_{ss} \quad \varepsilon^o_{\theta\theta} \quad \gamma^o_{s\theta}\}$, $(\boldsymbol{\kappa}^1)^{\mathrm{T}} = \{\kappa^1_s \quad \kappa^1_\theta \quad \kappa^1_{s\theta}\}$ and $(\boldsymbol{\gamma}^0)^{\mathrm{T}} = \{\gamma^o_{sz} \quad \gamma^o_{\theta z}\}$.

In shell analysis it is generally convenient to deal with the stress resultants and moment resultants rather than directly the stresses. Thus when each component of the stress vector, $\boldsymbol{\sigma}^{\mathrm{T}} = \{\sigma_{ss}\sigma_{\theta\theta}\tau_{\theta z}\tau_{sz}\tau_{s\theta}\}$, integrated over the thickness of the shell will comprise of the stress resultants and moment resultants, and these are referred through the generalized stress vector

represented as

$$\bar{\mathbf{N}}^* = \begin{Bmatrix} \bar{\mathbf{N}} \\ \bar{\mathbf{M}} \\ \bar{\mathbf{Q}} \end{Bmatrix},$$

where $\bar{\mathbf{N}}^{\mathrm{T}} = \{N_{ss} N_{\theta\theta} N_{s\theta}\}$, $\bar{\mathbf{M}}^{\mathrm{T}} = \{M_{ss} M_{\theta\theta} M_{s\theta}\}$, $\bar{\mathbf{Q}}^{\mathrm{T}} = \{Q_{ss} Q_{\theta\theta}\}$.

One can deduce from the figure that by setting the value of the principal radius of curvature R_ϕ equal to infinity, ϕ equal to 90° and the other principal radius of curvature R_θ equal to a finite radius equal to mean radius r, the geometry resembles a cylindrical shell. In the strain displacement equations, r, represents the parallel-circle radius to the shell mid-surface, can be inferred from Fig. 2 as equal to $r = R_\theta \sin\phi$. Considering these simplifications, the general strains displacement relations are used to formulate the stiffness and mass matrix.

A three-node isoparametric line element is used along the s-co-ordinate to generate the finite element mesh for the cylindrical shell (see Fig. 3). Each node has five-degrees-of-freedom. The element nodal d.o.f. are

$$\mathbf{d}^{\mathrm{T}} = \{u_1, v_1, w_1, \psi_{s1}, \psi_{\theta 1}, u_2, v_2, w_2, \psi_{s2}, \psi_{\theta 2}, u_3, v_3, w_3, \psi_{s3}, \psi_{\theta 3}\}. \tag{5}$$

The subscripts 1, 2 and 3 denote the node number. The shape functions N_i in terms of the isoparametric co-ordinate $\beta = (\bar{s}/l)$ (where $\bar{s}$ denotes the distance of a point on the element along the s-co-ordinate and l is length of the element) are given by

$$N_1 = \frac{(\beta^2 - \beta)}{2}, \quad N_2 = (1 - \beta^2) \text{ and } N_3 = \frac{(\beta^2 + \beta)}{2}. \tag{6a–c}$$

Displacement within the element are interpolated from element nodal d.o.f. vector $\mathbf{d}$,

$$\mathbf{u} = \mathbf{N}\mathbf{d}, \tag{7}$$

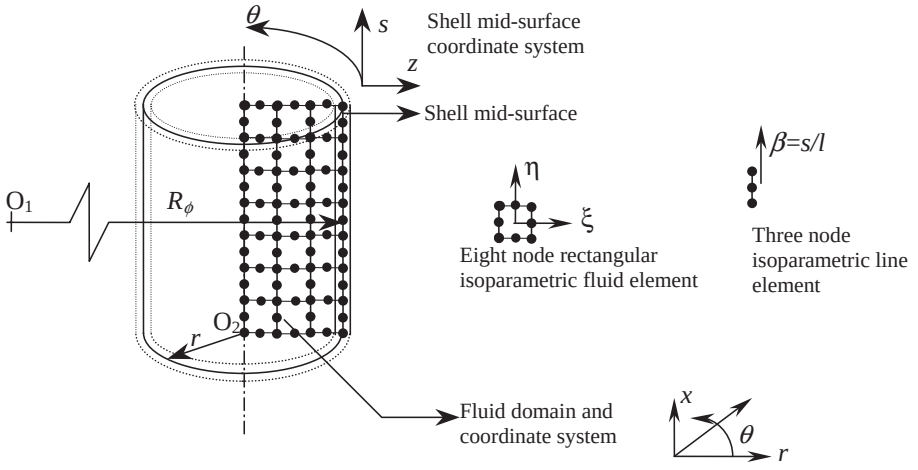

Fig. 3. Finite element mesh of the cylindrical shell and fluid domain.

where $\mathbf{u}^{\mathrm{T}} = \{u \quad v \quad w\}$. Strains are obtained from displacements by differentiation. Thus $\boldsymbol{\varepsilon} = [\partial]\mathbf{u}$ yields $\boldsymbol{\varepsilon} = \mathbf{B}^{*}\mathbf{d}$ where $\mathbf{B}^{*} = [\partial]\mathbf{N}$ and $[\partial]$ is the differential operator matrix given by the strain displacement relations.

The stress–strain relation for a shell lamina can be expressed as, $\boldsymbol{\sigma} = \bar{\bar{\mathbf{Q}}}^{*}\boldsymbol{\varepsilon}$.

$\bar{\bar{\mathbf{Q}}}^{*} = \mathbf{T}^{-1}\bar{\bar{\mathbf{Q}}}\mathbf{T}^{-\mathrm{T}}$ represents the transformed reduced stiffnesses where $\mathbf{T}^{-1}$ is the co-ordinate transformation matrix from the material co-ordinates to shell co-ordinates, $\bar{\bar{\mathbf{Q}}}$ denotes the reduced stiffnesses and the reader can refer to Jones [24] and Decolon [25] for details.

In case of shell analysis where one refers the strains with respect to the mid-surface, then the generalized stresses are related to the strains through the integrated shell stiffnesses as follows:

$$\begin{Bmatrix} \bar{\mathbf{N}} \\ \bar{\mathbf{M}} \\ \bar{\mathbf{Q}} \end{Bmatrix} = \begin{bmatrix} \mathbf{A} & \mathbf{B} & \mathbf{0} \\ \mathbf{B} & \mathbf{D} & \mathbf{0} \\ \mathbf{0} & \mathbf{0} & \mathbf{F} \end{bmatrix} \begin{Bmatrix} \boldsymbol{\varepsilon}^{\mathbf{0}} \\ \boldsymbol{\kappa}^{\mathbf{1}} \\ \boldsymbol{\gamma}^{\mathbf{0}} \end{Bmatrix}$$

or $\bar{\mathbf{N}}^{*} = \bar{\mathbf{D}}\boldsymbol{\varepsilon}$, the integrated transformed reduced shell stiffnesses are obtained as follows:

$$(A_{ij}, B_{ij}, D_{ij}, F_{ij}) = \int_{-(h/2)}^{+(h/2)} \bar{Q}_{ij}(1, z, z^2, z^3)\,\mathrm{d}z \tag{8}$$

$i = 1, 2$ and 6 and $j = 1, 2$ and 6. (Note: $\bar{Q}_{ij}$, tensorial notation, and $\bar{\bar{\mathbf{Q}}}$, matrix notation, mean the same.) A_{ij} are extensional stiffnesses, B_{ij} are the bending-extensional coupling stiffnesses, D_{ij} are bending stiffnesses and F_{ij} are thickness shear stiffnesses. The stiffness matrix is obtained from the strain energy as

$$U_1 = \tfrac{1}{2}\mathbf{d}^{\mathrm{T}}\mathbf{k}_e\mathbf{d}.$$

where $\mathbf{k}_e$ is the element stiffness matrix corresponding to the mth harmonic and is computed as follows:

$$\mathbf{k}_e = \int_A \mathbf{B}^{*\mathbf{T}}\bar{\mathbf{D}}\mathbf{B}^{*} r\,\mathrm{d}s\,\mathrm{d}\theta, \tag{9}$$

where $\mathbf{B}^{*}$ is the strain-displacement matrix of the shell at stress free temperature T_o. The element stiffness matrix is assembled using standard assembly procedure in finite element analysis to obtain the global stiffness matrix, $\mathbf{K}^{uu} = \sum \mathbf{k}_e$. Due to orthogonality principle the stiffness matrix become decoupled for each circumferential harmonic.

The constitutive matrix $\bar{\mathbf{D}}$ in Eq. (9) consisting of various integrated shell stiffnesses: A_{ij}, B_{ij}, D_{ij}, and F_{ij}. Shear correction factor equal to 5/6 is used.

3.1.2. Geometric stiffness matrix

Zienckiewicz and Taylor [26] describe a finite element method to deal with geometrically non-linear problems which will be useful in dealing with the classical 'initial' stability problem. A detailed discussion is presented to evaluate the geometric stiffness matrix based on the initial stresses for plates and shells. Accordingly in the present work, the effect of initial stresses developed due to temperature is used to evaluate the geometric stiffness matrix. To start with the stresses σ^{*}_{ss}, $\sigma^{*}_{\theta\theta}$ and $\tau^{*}_{s\theta}$ are obtained by accounting the thermal effects. Strain energy due to initial stresses U_2 neglecting the strain energy due to initial transverse shear stresses is given in

Ramalingeswara Rao [27] as

$$U_2 = \frac{1}{2}\int_V \{\, \varepsilon^i_{ss} \quad \varepsilon^i_{\theta\theta} \,\} \begin{bmatrix} \sigma^*_{ss} & \tau^*_{s\theta} \\ \tau^*_{s\theta} & \sigma^*_{\theta\theta} \end{bmatrix} \begin{Bmatrix} \varepsilon^i_{ss} \\ \varepsilon^i_{\theta\theta} \end{Bmatrix} \mathrm{d}V, \tag{10}$$

$$U_2 = \frac{1}{2}\int_V \{(\varepsilon^i_{ss})^2\sigma^*_{ss} + (\varepsilon^i_{\theta\theta})^2\sigma^*_{\theta\theta} + 2\gamma^i_{s\theta}\tau^*_{s\theta}\}\, \mathrm{d}V,$$

where σ^*_{ss}, $\sigma^*_{\theta\theta}$ and $\tau^*_{s\theta}$ are the initial stresses which are constant and depend on temperature rise ΔT. ε^i_{ss}, $\varepsilon^i_{\theta\theta}$ and $\gamma^i_{s\theta}$ are given as follows:

$$\varepsilon^i_{ss} = \frac{1}{(1+z/R_\phi)}\left(\frac{\partial w^i}{\partial s} - \frac{u^i}{R_\phi}\right), \tag{11a}$$

$$\varepsilon^i_{\theta\theta} = \frac{1}{(1+z/R_\theta)}\left(\frac{1}{r}\frac{\partial w^i}{\partial \theta} - \frac{v^i}{r}\sin\phi\right), \tag{11b}$$

$$\gamma^i_{s\theta} = \varepsilon^i_{ss}\varepsilon^i_{\theta\theta} \tag{11c}$$

z is the thickness quantity of the shell measured along the z co-ordinate and the superscripts 'i' denote the quantities due to temperature effects. Based on the usual manipulation in finite element procedure Eq. (10) can be put in the following form for a finite element as

$$U_2 = \tfrac{1}{2}\mathbf{d}^{i\mathrm{T}}\mathbf{k}_{\sigma e}\,\mathbf{d}^i \tag{12}$$

$\mathbf{d}^i$ is the element d.o.f. as indicated in Eq. (5), but these quantities are due to thermal effects. The matrix $\mathbf{k}_{\sigma e}$ in the foregoing equation is the element geometric stiffness matrix

$$\mathbf{k}_{\sigma e} = \int_V \mathbf{B}^{i\mathrm{T}}\boldsymbol{\sigma}^*\,\mathbf{B}^i \mathrm{d}V,$$

$$\mathbf{k}_{\sigma e} = \int_A \mathbf{B}^{i\mathrm{T}}\bar{\mathbf{N}}^{th}\,\mathbf{B}^i \mathrm{d}A, \tag{13}$$

$\mathbf{B}^i$ is the strain displacement matrix based on Eqs. (11a)–(11c) and $\{\boldsymbol{\sigma}^*\}$ is the matrix comprising of the initial stresses due to thermal load and for shell analysis it is equivalent to $\bar{\mathbf{N}}^{th^{\mathrm{T}}} = \{\,\mathbf{N}^* \quad \mathbf{M}^* \quad \mathbf{Q}^*\,\}$ is a matrix of initial stress and moment resultants. Assembling the element geometric stiffness matrix yields global geometric stiffness matrix, $\mathbf{K}^{uu}_{\sigma} = \sum \mathbf{k}_{\sigma e}$. The computational procedure of initial stress resultants and moment resultants, $\bar{\mathbf{N}}^{th}$, is described in next section.

3.1.3. Thermal load and initial stress evaluation

The temperature is assumed to be constant over the thickness and the temperature field for the shell continuum is $T(s,\theta,z,t) = T(s,\theta,t)$. Fourier series is used to express the steady state temperature in the circumferential direction,

$$T(s,\theta,t) = \sum_{m=0}^{\infty} T_m(s,t)\cos m\theta$$

the subscript 'm' indicates the harmonic number (or circumferential mode number). Under thermal environment the expression for the total potential is as follows:

$$\Pi = \frac{1}{2}\int_V \boldsymbol{\varepsilon}^{\mathrm{T}}\bar{\mathbf{C}}\boldsymbol{\varepsilon}\,\mathrm{d}V - \int_V \boldsymbol{\varepsilon}^{\mathrm{T}}\bar{\mathbf{C}}\boldsymbol{\varepsilon}_o\,\mathrm{d}V + \frac{1}{2}\int_V \boldsymbol{\varepsilon}_o^{\mathrm{T}}\bar{\mathbf{C}}\boldsymbol{\varepsilon}_o\,\mathrm{d}V$$

where $\bar{\mathbf{C}}$ is the elastic matrix and $\boldsymbol{\varepsilon}_\mathbf{o}$ is the strain due to temperature effects. In the above expression the third term drops out as a result of minimization of the total potential energy. Since the strains are referred to the mid-surface of the shell, the above expression can be rewritten for analysis of shells as

$$\Pi = \frac{1}{2}\int_A \boldsymbol{\varepsilon}^{\mathrm{T}}\bar{\mathbf{D}}\boldsymbol{\varepsilon}\,\mathrm{d}A - \int_A \boldsymbol{\varepsilon}^{\mathbf{T}}\boldsymbol{\lambda}\,\mathrm{d}A. \tag{14}$$

Minimization of Π with respect to the displacement vector $\mathbf{d}^{th}$ yields the standard equilibrium equation for finite element of the shell continuum, $\mathbf{k}_e\mathbf{d}^{th} - \mathbf{F}_e^{th} = 0$, where $\mathbf{k}_e$ is the element stiffness matrix computed as described in Eq. (9), $\mathbf{d}^{th}$ is the element displacement vector due to temperature effects and $\mathbf{F}_e^{th}$ is the element thermal load vector. On assembling the element matrix and element vectors we obtain the global matrix and vectors, hence

$$\mathbf{K}^{uu}\mathbf{d}_g^{th} - \mathbf{F}^{th} = 0 \tag{15}$$

$\mathbf{K}^{uu}$ is the global stiffness matrix and $\mathbf{d}_g^{th}$, and $\mathbf{F}^{th}$ global displacement vector and global thermal load vector respectively. ΔT denote the temperature rise from the stress free temperature, T_o. The second term in the above, Eq. (15), denotes the thermal loading on the structure and evaluated as follows:

$$\mathbf{F}^{th} = \int_A \boldsymbol{\varepsilon}^{\mathrm{T}}\boldsymbol{\lambda}\,\mathrm{d}A, \tag{16}$$

where $\boldsymbol{\lambda}$ is the temperature stress coefficients computed for the shell lamina as

$$\boldsymbol{\lambda} = \bar{\mathbf{D}}^*\bar{\boldsymbol{\alpha}}\Delta T(z) \tag{17}$$

$\bar{\mathbf{D}}^* = \int_{-h/2}^{h/2}\bar{Q}_{ij}(1,z)\,\mathrm{d}z$, comprising of the stiffnesses: A_{ij}, and B_{ij}, where $i,j = 1,2$ and 6.

The coefficient of thermal expansion for shell co-ordinate system is: $\bar{\boldsymbol{\alpha}}^{\mathrm{T}} = \{\alpha_s\alpha_\theta\alpha_{s\theta}\alpha_s\alpha_\theta\alpha_{s\theta}00\}$, where α_s and α_θ are the coefficients of thermal expansion in the directions parallel and perpendicular to the material co-ordinate axis.

Using Eq. (16) the thermal load is computed for a steady state axisymmetric temperature, above the stress free temperature T_o, which is assumed to be 20°C. Solving Eq. (15) gives the displacement field, $\mathbf{d}_g^{th}$, due to the thermal loading and thereby the strains $\boldsymbol{\varepsilon}_o$. Following the procedure described in Cook et al. [28] related to the computation of stresses due to thermal loading, the stress resultants will be the sum of the mechanical stress resultants due to thermal load and the stress resultants due to temperature rise.

$$\bar{\mathbf{N}}^{th} = \bar{\mathbf{D}}\boldsymbol{\varepsilon}_o - \boldsymbol{\lambda} \tag{18}$$

$\boldsymbol{\varepsilon}_o$ represents the strain developed in the structural continuum due to thermal load, $\bar{\mathbf{D}}$, is a matrix comprising of various integrated reduced shell stiffnesses in the transformed co-ordinate, and $\boldsymbol{\lambda}$ represents the temperature stress coefficients, and is computed as described in Eq. (17). The stress resultants and moment resultants are found for each finite element and are used in Eq. (13) to compute the element geometric stiffness matrix.

3.1.4. Mass matrix

The mass matrix is obtained from the kinetic energy of the shell continuum,

$$KE = \frac{\rho_s}{2}\int_V (\dot{u}^2 + \dot{v}^2 + \dot{w}^2)\,\mathrm{d}V = \frac{\rho_s}{2}\int_V \mathbf{u}^{\mathrm{T}}\mathbf{u}\,\mathrm{d}V$$

ρ_s is the density of shell material. Using Eq. (7) the kinetic energy will be

$$KE = \tfrac{1}{2}\mathbf{d}^{\mathrm{T}}\mathbf{m}_e\mathbf{d},$$

where $\boldsymbol{m}_e$ is the element mass matrix given by

$$\mathbf{m}_e = \rho_s \int_V \mathbf{N}^{\mathrm{T}}\mathbf{N}\,\mathrm{d}V \tag{19}$$

Fig. 3 illustrates the typical discretization procedure suitable for semi-analytical finite method. The cylindrical shell uses a three node isoparametric line element and the fluid domain uses an annular eight node rectangular isoparametric element, Ross [29].

3.2. Finite element formulation for incompressible fluid flow

The fluid–structure interaction is described by linear potential flow theory. The hot fluid flowing internal to the shell is assumed to be incompressible and non-viscous. The flow is isentropic and irrotational. The hot fluid always remains adhered to the internal wall of the shell and the fluid pressure acts normal to the wall of the shell. Velocity potential is considered as the nodal degree of freedom in the fluid finite element and it is required that the velocity potential satisfy the Laplace equation. The fluid element is a rectangular isoparametric element with eight nodes (see Fig. 3).

The governing differential equation for the irrotational steady flow of fluid through the shell is the Laplace equation

$$\nabla^2\bar{\phi} = 0, \tag{20}$$

where $\bar{\phi}$ is the velocity potential. In cylindrical co-ordinates the Laplace equation is

$$\frac{1}{r}(r\bar{\phi}_{,r})_{,r} + \frac{1}{r^2}\bar{\phi}_{,\theta\theta} + \bar{\phi}_{,xx} = 0. \tag{21}$$

The flow of fluid through the cylindrical shell is composed of two components. One component of velocity is due to steady flow and the second velocity component is associated with the vibrations of the shell wall, referred to as perturbation velocity. The perturbation velocity components are expressed as function of velocity potential. Thus the total velocity V_x, V_θ and V_r in the axial, tangential and radial directions are

$$V_x = U_x + \bar{\phi}_{,x}, \quad V_\theta = \frac{1}{R}\bar{\phi}_{,\theta}, \quad V_r = \bar{\phi}_{,r}$$

U_x is the steady state mean axial flow velocity of the fluid.

Bernoulli's equation for the unsteady flow case is used to compute the dynamic pressure, p, acting on the shell surface and can be deduced as

$$p = -\rho(\bar{\phi}_{,t} + U_x\bar{\phi}_{,x}). \tag{22}$$

The impermeability condition will assure the fluid–structure interface coupling. One way to account for the impermeability condition is to assume that the instantaneous normal velocity (or radial velocity) of fluid is equal to the radial velocity of the shell. The kinematic boundary condition is expressed through the following relationship:

$$V_r = \bar{\phi}_{,r}\big|_{r=R} = \frac{\mathrm{D}w}{\mathrm{D}t} = w_{,t} + U_x w_{,x}, \tag{23}$$

where w denotes the normal displacement component of the shell surface (z-co-ordinate). The second term in the Eq. (23) $U_x w_{,x}$ represents the velocity of the fluid due to local change of slope, Lakis et al. [30].

Galerkin's weighted residual approach is used to formulate the finite element form of the governing Laplace equation. The weighting function used is the fluid shape functions N_f which are described in Ross [29].

$$\int_V N_f^{\mathrm{T}} \nabla^2 \bar{\phi}\, \mathrm{d}V = 0,$$

$$\int_S N_f^{\mathrm{T}} \nabla \bar{\phi} \cdot \mathbf{n}\, \mathrm{d}S - \int_V \nabla N_f^{\mathrm{T}} \nabla \bar{\phi}\, \mathrm{d}V = 0, \tag{24}$$

$\mathbf{n}$ is the unit normal vector to the structure. In the above equation,

$$\nabla \bar{\phi} \cdot \mathbf{n} \equiv \frac{\partial \bar{\phi}}{\partial r} = \frac{\mathrm{D}w(x,\theta,r,t)}{\mathrm{D}t} = \frac{\partial w}{\partial t} + U_x \frac{\partial w}{\partial x} + U_\theta \frac{\partial w}{\partial \theta} + U_r \frac{\partial w}{\partial r}.$$

The nature of flow through the shell is assumed as plug flow (i.e., uniform velocity profile across the cross-section of the shell). The components of velocity U_r and U_θ will be zero, hence

$$\nabla \bar{\phi} \cdot \mathrm{n} = \frac{\partial w}{\partial t} + U_x \frac{\partial w}{\partial x}.$$

In the semi-analytical method we assume the velocity potential to be dependent in the circumferential direction and is expressed using the Fourier series as

$$\bar{\phi}(x,\theta,r,t) = \sum_{m=0}^{\infty} \bar{\phi}(x,r,t) \cos m\theta.$$

The velocity potential for a fluid finite element is expressed using the fluid shape function as

$$\bar{\phi}_e(x,\theta,r,t) = \sum_{i=1}^{fnodes} \sum_{m=0}^{\infty} N_{fi} \bar{\phi}_i(x,r,t) \cos m\theta$$

and using the structural shape functions, N, Eq. (24) is rewritten as follows:

$$\int N_f^{\mathrm{T}} N\, \mathrm{d}S\{\dot{U}_e\} + U_x \int N_f^{\mathrm{T}} \frac{\partial N}{\partial x}\, \mathrm{d}S\{U_e\} - \int_V \nabla N_f^{\mathrm{T}} \nabla N_f\, \mathrm{d}V. \tag{25}$$

The first two terms in Eq. (25) yields the fluid–structure coupling terms namely, $\mathbf{C}_e^{\phi u}$ and $\mathbf{K}_e^{\phi u}$. In evaluating these matrices 'w' component of shell displacement alone will be involved in computation. $w(s,\theta,z,t) = \sum_{i=1}^{snodes} \sum_{m=0}^{\infty} N_i w_{mi}(s,z,t) \cos m\theta$ where $i = 1$, *snodes* indicate the number of nodes of the shell finite element interacting with the fluid finite element nodes. The

third term indicates the kinetic energy of the fluid finite element, $\mathbf{H}_e^{\phi\phi}$. The subscript 'e' stands for element matrix.

Again applying the Galerkin's weighted residual procedure to Eq. (22), the fluid–structure coupling terms viz. $\mathbf{C}_e^{u\phi}$ and $\mathbf{K}_e^{u\phi}$ can be obtained as follows:

$$\int_S N^{\mathrm{T}}\rho_f(\bar{\phi}_{,t}+U_x\bar{\phi}_{,x})\,\mathrm{d}S=\rho_f\int_S N^{\mathrm{T}}N_f\,\mathrm{d}S\{(\bar{\phi}_{,t})_e\}+\rho_f U_x\int_S N^{\mathrm{T}}\frac{\partial N_f}{\partial x}\,\mathrm{d}S\{\bar{\phi}_e\}.$$

Considering the global finite element matrices namely the mass matrix, stiffness matrix of the cylindrical shell, the geometric stiffness matrix due to axisymmetric temperature, global fluid–structure coupling terms and the kinetic energy of the fluid, the equation governing the motion of the coupled fluid–structure system under thermal loading due to steady flow of fluid at uniform temperature in global co-ordinates is written as follows:

$$\begin{bmatrix}\mathbf{M}^{uu} & \mathbf{0}\\ \mathbf{0} & \mathbf{0}\end{bmatrix}\begin{Bmatrix}\ddot{\mathbf{u}}\\ \ddot{\bar{\phi}}\end{Bmatrix}+\begin{bmatrix}\mathbf{0} & \mathbf{C}^{u\phi}\\ -\mathbf{C}^{\phi u} & \mathbf{0}\end{bmatrix}\begin{Bmatrix}\dot{\mathbf{u}}\\ \dot{\bar{\phi}}\end{Bmatrix}+\begin{bmatrix}\mathbf{K}^{uu}+\mathbf{K}_\sigma^{uu} & U_x\mathbf{K}^{u\phi}\\ -U_x\mathbf{K}^{\phi u} & \mathbf{H}^{\phi\phi}\end{bmatrix}\begin{Bmatrix}\mathbf{u}\\ \bar{\phi}\end{Bmatrix}=0. \tag{26}$$

Further we proceed to condense the fluid equation as follows:

$$-\mathbf{C}^{\phi u}\dot{\mathbf{u}}-U_x\mathbf{K}^{\phi u}\mathbf{u}+\mathbf{H}^{\phi\phi}\bar{\phi}=0,$$

$$\bar{\phi}=\mathbf{H}^{\phi\phi-1}\mathbf{C}^{\phi u}\dot{\mathbf{u}}+U_x\mathbf{H}^{\phi\phi-1}\mathbf{K}^{\phi u}\mathbf{u},$$

$$\dot{\bar{\phi}}=\mathbf{H}^{\phi\phi-1}\mathbf{C}^{\phi u}\ddot{\mathbf{u}}+U_x\mathbf{H}^{\phi\phi-1}\mathbf{K}^{\phi u}\dot{\mathbf{u}}.$$

Substituting $\bar{\phi}$ and $\dot{\bar{\phi}}$ in the structural equation (Eq. (26)), we get

$$\begin{aligned}&(\mathbf{M}^{uu}+\mathbf{C}^{u\phi}\mathbf{H}^{\phi\phi^{-1}}\mathbf{C}^{\phi u})\ddot{\mathbf{u}}+U_x(\mathbf{C}^{u\phi}\mathbf{H}^{\phi\phi^{-1}}\mathbf{K}^{\phi u}+\mathbf{K}^{u\phi}\mathbf{H}^{\phi\phi^{-1}}\mathbf{C}^{\phi u})\dot{\mathbf{u}}\\&+(\mathbf{K}^{uu}+\mathbf{K}_\sigma^{uu}+U_x^2\mathbf{K}^{u\phi}\mathbf{H}^{\phi\phi^{-1}}\mathbf{K}^{\phi u})\mathbf{u}=0,\end{aligned} \tag{27a}$$

$$\mathbf{M}^*\ddot{\mathbf{u}}+\mathbf{C}^*\dot{\mathbf{u}}+\mathbf{K}^*\mathbf{u}=0, \tag{27b}$$

where $\mathbf{M}^*=(\mathbf{M}^{uu}+\mathbf{C}^{u\phi}\mathbf{H}^{\phi\phi^{-1}}\mathbf{C}^{\phi u})$; $\mathbf{C}^*=U_x(\mathbf{C}^{u\phi}\mathbf{H}^{\phi\phi^{-1}}\mathbf{K}^{\phi u}+\mathbf{K}^{u\phi}\mathbf{H}^{\phi\phi^{-1}}\mathbf{C}^{\phi u})$; $\mathbf{K}^{**}=(\mathbf{K}^{uu}+\mathbf{K}_\sigma^{uu})$; $\mathbf{K}_a=U_x^2(\mathbf{K}^{u\phi}\mathbf{H}^{\phi\phi^{-1}}\mathbf{K}^{\phi u})$ and $\mathbf{K}^*=\mathbf{K}^{**}+\mathbf{K}_a$, $\mathbf{C}^{u\phi}\mathbf{H}^{\phi\phi}\mathbf{C}^{\phi u}$, is the added mass term; $\mathbf{C}^{u\phi}\mathbf{H}^{\phi\phi^{-1}}\mathbf{K}^{\phi u}+\mathbf{K}^{u\phi}\mathbf{H}^{\phi\phi^{-1}}\mathbf{C}^{\phi u}$ is called the added damping term due to potential formulation and $\mathbf{K}^{u\phi}\mathbf{H}^{\phi\phi^{-1}}\mathbf{K}^{\phi u}$ is the added stiffness term due to stiffening by the pressure acting on the walls.

Eq. (27b) can be written in the state space form by letting $\mathbf{a}=\begin{Bmatrix}u\\ \dot{u}\end{Bmatrix}$ as follows:

$$\omega\begin{bmatrix}-\mathbf{C}^* & -\mathbf{M}^*\\ \mathbf{M}^* & \mathbf{0}\end{bmatrix}\mathbf{a}=\begin{bmatrix}\mathbf{K}^* & \mathbf{0}\\ \mathbf{0} & \mathbf{M}^*\end{bmatrix}\mathbf{a}. \tag{28}$$

The above equation can be used to study the dynamics of shells conveying a steady flow of hot fluid at a steady state temperature, the fluid being incompressible and inviscid. ω (rad/s) is the natural frequency of the coupled system for a given steady flow velocity of the fluid and steady state temperature of the fluid.

Many investigations are reported in the literature on the dynamic stability of pipes/shells conveying pulsating fluid and generally the flow velocity is assumed in the following form,

$$U_x = U_o(1 + \mu \cos \Omega t), \tag{29}$$

consisting of the harmonically varying term superposed on the mean flow velocity. U_o is the mean flow velocity, μ represents the excitation parameter (μU_o is the amplitude of perturbation), Ω is the pulsating frequency of flow and t the time. Substituting Eq. (29) into Eq. (27a) the dynamic equation of motion describing the behavior of shell containing the flow of a pulsatile fluid is

$$\mathbf{M}^*\ddot{\mathbf{u}} + U_o\mathbf{C}^*\dot{\mathbf{u}} + \left(\mathbf{K}^{**} + U_o^2\left(1 + \frac{\mu^2}{2}\right)\mathbf{K}_a\right)\mathbf{u} + U_o\mu \cos \Omega t\, \mathbf{C}^*\dot{\mathbf{u}} + U_o^2\mu\left(2 \cos \Omega t + \frac{\mu}{2}\cos 2\Omega t - \frac{\Omega}{U_o}\sin \Omega t\right)\mathbf{K}_a\mathbf{u} = 0. \tag{30}$$

In the above equation the damping term and stiffness term (excluding the geometric stiffness matrix) are time-dependent. In the next section we discuss the solution methodology to solve the system of periodic equations.

3.3. Stability analysis: Floquet–Liapanov theory, fourth order Runge–Kutta method, Gill's coefficient

The most general method to solve the differential equations with periodic coefficients is the theory of Floquet–Liapanov. According to this theorem, the knowledge of the state transition matrix over one period is sufficient to determine the stability of the system. This theory involves the computation of the state transition matrix. Freidman et al. [22] describe another methodology for evaluating the state transition matrix with less computation time involved. This is due to the fact that the state transition is independent of the initial conditions, hence proposed a new numerical integration method to obtain the state transition matrix in single pass integration. This new integration scheme is based on the fourth order Runge–Kutta method and makes use of Gill coefficient. This method is beneficial for large system which obviously cuts down huge computational time.

The methodology developed by Friedmann and Hammond is discussed in this paper. Consider the general differential equation of motion, Eq. (30) which describes the behavior of a shell conveying a pulsatile flow. For the sake of simplicity we write Eq. (30) as follows (i.e., equation of motion with time-dependent coefficient):

$$\mathbf{M}\ddot{\mathbf{u}} + \mathbf{C}(t)\dot{\mathbf{u}} + \mathbf{K}(t)\mathbf{u} = 0. \tag{31}$$

In the state space form the equation is

$$\dot{\mathbf{b}} = \bar{\mathbf{A}}(t)\mathbf{b} = \{f(t, \mathbf{b})\}, \tag{32}$$

where

$$\bar{\mathbf{A}}(t) = \begin{bmatrix} 0 & \mathbf{I} \\ -\mathbf{M}^{-1}\mathbf{K} & -\mathbf{M}^{-1}\mathbf{C} \end{bmatrix}, \quad \mathbf{b} = \begin{Bmatrix} u \\ \dot{u} \end{Bmatrix}.$$

In Eq. (32), $\bar{\mathbf{A}}(t) = \bar{\mathbf{A}}(t + T_p)$and t is time co-ordinate and T_p is the time period.

The transition matrix can be written as $[\Phi(t,t_0)] = [P(t)]^{-1}\exp[R(t-t_0)][P(t_0)]$ where $[P(t+T_p)] = [P(t)]$ is the periodic matrix and $[R]$ is a constant matrix, given by the relation $[\Phi(T_p,0)] = \exp([R]T_p)$. The knowledge of the transition matrix over one period determines the solution to the homogeneous system everywhere through the relation $[\Phi(t+iT_p,0)] = [\Phi(t,0)](\exp([R]T_p))^i$ where $0 \leqslant t \leqslant T_p$ and i is any integer. The stability criteria for the system are related to the eigenvalues of $[R]$ or the real part of the characteristic exponents. The solution of Eq. (32) approach zero as $t \to \infty$ if all the eigenvalues of $[R]$ is less than 1 and otherwise the system is not stable.

The fourth order Runge–Kutta method with Gill coefficients is given by

$$\mathbf{b}_{i+1} = \mathbf{b}_i + \frac{h_t}{6}\left(\mathbf{k}_1 + 2\left(1-\frac{1}{\sqrt{2}}\right)\mathbf{k}_2 + 2\left(1+\frac{1}{\sqrt{2}}\right)\mathbf{k}_3 + \mathbf{k}_4\right), \tag{33}$$

where $\mathbf{b}_i = \mathbf{b}(t_i)$, i is the ith interval and $h_t = t_{i+1} - t_i$ is the step size. The vectors $\mathbf{k}_1, \mathbf{k}_2, \mathbf{k}_3$ and $\mathbf{k}_4$ are given by

$$\mathbf{k}_1 = \{f(t_i, \mathbf{b}_i)\}, \tag{34}$$

$$\mathbf{k}_2 = \left\{f\left(\left(t_i + \frac{1}{2}h_t\right), \mathbf{b}_i + \frac{1}{2}\mathbf{k}_1\right)\right\}, \tag{35}$$

$$\mathbf{k}_3 = \left\{f\left(\left(t_i + \frac{1}{2}h_t\right), \mathbf{b}_i + \left(-\frac{1}{2}+\frac{1}{\sqrt{2}}\right)h_t\mathbf{k}_1 + \left(1-\frac{1}{\sqrt{2}}\right)h_t\mathbf{k}_2\right)\right\}, \tag{36}$$

$$\mathbf{k}_4 = \left\{f\left((t_i + h_t), \mathbf{b}_i - \frac{1}{\sqrt{2}}h_t\mathbf{k}_2 + \left(1+\frac{1}{\sqrt{2}}\right)h_t\mathbf{k}_3\right)\right\}. \tag{37}$$

Combining Eqs. (32) and (34)–(37) will result in

$$\mathbf{k}_1 = \bar{\mathbf{A}}(t_i)\mathbf{b}_i, \tag{38}$$

$$\mathbf{k}_2 = \bar{\mathbf{E}}(t_i)\mathbf{b}_i, \tag{39}$$

$$\mathbf{k}_3 = \bar{\mathbf{F}}(t_i)\mathbf{b}_i, \tag{40}$$

$$\mathbf{k}_4 = \bar{\mathbf{G}}(t_i)\mathbf{b}_i, \tag{41}$$

where

$$\bar{\mathbf{E}}(t_i) = \bar{\mathbf{A}}\left(t_i + \frac{h_t}{2}\right)\left(\mathbf{I} + \frac{1}{2}h_t\bar{\mathbf{A}}(t_i)\right), \tag{42}$$

$$\bar{\mathbf{F}}(t_i) = \bar{\mathbf{A}}\left(t_i + \frac{h_t}{2}\right)\left(\mathbf{I} + \left(-\frac{1}{2}+\frac{1}{\sqrt{2}}\right)h_t\bar{\mathbf{A}}(t_i) + \left(1-\frac{1}{\sqrt{2}}\right)h_t\bar{\mathbf{E}}(t_i)\right), \tag{43}$$

$$\bar{\mathbf{G}}(t_i) = (\bar{\mathbf{A}}(t_i + h_t))\left(\mathbf{I} - \frac{h_t}{\sqrt{2}}\bar{\mathbf{E}}(t_i) + \left(1+\frac{1}{\sqrt{2}}\right)h_t\bar{\mathbf{F}}(t_i)\right). \tag{44}$$

Combining Eqs. (33) and (38)–(41) and Eqs. (42)–(44) gives

$$\mathbf{b}_{i+1} = \bar{\mathbf{B}}(t_i)\mathbf{b}_i, \tag{45}$$

where

$$\bar{\mathbf{B}}(t_i) = \mathbf{I} + \frac{h_t}{6}\left(\bar{\mathbf{A}}(t_i) + 2\left(1 - \frac{1}{\sqrt{2}}\right)\bar{\mathbf{E}}(t_i) + 2\left(1 + \frac{1}{\sqrt{2}}\right)\bar{\mathbf{F}}(t_i) + \bar{\mathbf{G}}(t_i)\right). \tag{46}$$

Using Eq. (45) the following expressions can be written out

$$\mathbf{b}(t_1) = \bar{\mathbf{B}}(t_0)\mathbf{b}(t_0),$$

$$\mathbf{b}(t_2) = \bar{\mathbf{B}}(t_1)\mathbf{b}(t_1) = \bar{\mathbf{B}}(t_1)\bar{\mathbf{B}}(t_0)\mathbf{b}(t_0),$$

$$\mathbf{b}(t_n) = \bar{\mathbf{B}}(t_{n-1})\bar{\mathbf{B}}(t_{n-2})\ldots\bar{\mathbf{B}}(t_0)\mathbf{b}(t_0).$$

For constant step size $h_t = T_p/N_{tsdivi}$ with $t_0 = 0$ and $t_n = T_p$, the last of the above equation reduces to

$$\begin{aligned}\mathbf{b}(T_p) &= \bar{\mathbf{B}}(T_p - h_t)\bar{\mathbf{B}}(T_p - 2h_t)\ldots\bar{\mathbf{B}}(0)\mathbf{b}(0)\\ &= \left(\prod_{i=1}^{N}\bar{\mathbf{B}}(T_p - ih_t)\right)\mathbf{b}(0)\\ &= \Phi_A(T_p, 0)\mathbf{b}(0).\end{aligned} \tag{47}$$

Thus, the approximate transition matrix at the end of a period obtained by one integration pass is

$$\Phi_A(T_p, 0) = \prod_{i=1}^{N_{tsdiv}}\bar{\mathbf{B}}(T_p - ih_t). \tag{48}$$

3.4. Modal reduction for stability analysis

It has been discussed in the recently published work by Jayaraj et al. [19] the difficulties involved as a result of using the method suggested by Friedmann and Hammond [22] for stability analysis. This method outline above for the computation of the state transition matrix involves a large number of multiplications which can lead to overflow errors. This is especially true in case of large finite element model involved in the study of parametric instability. The method suggested by Jayaraj et al. [19] is to reduce the size of the problem and one way of achieving this in dynamic analysis problems is by transforming the problem into a modal domain. In doing so it should be borne in mind that the stability information should be retained in the reduced set of equations. This is possible only when one considers the linear transformation. The co-ordinate transformation to the modal domain is made using the first few eigenvectors of the time invariant system. Here we consider the free vibration mode shape of the cylindrical shell with steady flow of fluid. These are obtained using the finite element equation for the cylindrical shell with a steady flow of fluid with no damping, and this is reduced from Eq. (30) as

$$\mathbf{M}^*\ddot{\mathbf{u}} + \left(\mathbf{K}^* + U_0^2\left(1 + \frac{\mu^2}{2}\right)\mathbf{K}_a\right)\mathbf{u} = 0. \tag{49}$$

Using the LAPACK's [31] routine RGG, the eigenvectors φ of Eq. (49) are found. These eigenvectors are orthogonal with respect to $\mathbf{M}^*$ and $(\mathbf{K}^* + U_0^2(1 + (\mu^2/2))\mathbf{K}_a)$. Using the transformation $\mathbf{u} = \varphi\mathbf{y}$ in the full Eq. (30) and pre-multiplying by φ^{T}

$$\varphi^{\mathrm{T}}\mathbf{M}^*\varphi\ddot{\mathbf{y}} + U_0\varphi^{\mathrm{T}}\mathbf{C}^*\varphi\dot{\mathbf{y}} + \varphi^{\mathrm{T}}\left(\mathbf{K}^* + U_o^2\left(1 + \frac{\mu^2}{2}\right)\mathbf{K}_a\right)\varphi\mathbf{y} + U_0\mu\cos\Omega t\varphi^{\mathrm{T}}\mathbf{C}^*\varphi\dot{\mathbf{y}} + U_0^2\mu\left(2\cos\Omega t + \frac{\mu}{2}\cos 2\Omega t - \frac{\Omega}{U_o}\sin\Omega t\right)\varphi^{\mathrm{T}}\mathbf{K}_a\varphi\mathbf{y} = 0.$$

The resulting matrix can be written as

$$\mathbf{M}^r\ddot{\mathbf{y}} + \mathbf{C}^r(t)\dot{\mathbf{y}} + \mathbf{K}^r(t)\mathbf{y} = 0, \tag{50}$$

where $\mathbf{M}^r = \varphi^{\mathrm{T}}\mathbf{M}\varphi = \mathbf{I}$, $\mathbf{C}^r(t) = U_0(1 + \mu\cos\Omega t)\varphi^{\mathrm{T}}\mathbf{C}^*\varphi$ and

$$\mathbf{K}^r(t) = \varphi^{\mathrm{T}}\left(\mathbf{K}^* + U_0^2\left(1 + \frac{\mu^2}{2} + 2\mu\cos\Omega t + \frac{\mu^2}{2}\cos 2\Omega t - \frac{\mu}{U_o}\Omega\sin\Omega t\right)\mathbf{K}_a\right)\varphi.$$

Here the mass matrix $\mathbf{M}^r$ is diagonal and is the identity matrix, but $\mathbf{C}^r(t)$ and $\mathbf{K}^r(t)$ are not diagonal matrices. However, the matrices are now considerably smaller when compared to the original problem. Due to these reasons the numerical computation should not pose any difficulties. In the normalization process, the stiffness coefficients become much smaller (from $O(10^9)$ to $O(10^3)$ and mass coefficients from $O(10^{-3})$ to $O(1)$, based on the studies by Jayaraj et al. [19].

4. Numerical results and discussions

Computation of the parametric instability regions are carried out for a typical cylindrical shell with $l/r = 1.048$ and clamped–clamped boundary condition. The overall computation work involves the determination of (i) lowest thermal buckling temperature for various circumferential modes, (ii) under steady flow of fluid, determining the critical mean axial flow velocity and finally (iii) the instability regions that results due to flow of pulsatile fluid through the shell. The computational results are discussed in separate sections below.

4.1. Thermal buckling temperature evaluation

Knowledge of the critical thermal buckling temperature is essential to start the study on dynamic stability of cylindrical shells containing the flow of hot water which is periodically varying with time. The buckling temperature of the cylindrical shell under axisymmetric temperature variation will give an indication for the maximum fluid temperature that is permitted for analysis. We make use of Eq. (26) in the uncoupled form: $(\mathbf{K}^{uu} + \chi\mathbf{K}_\sigma^{uu})\mathbf{u}_b = 0$, where $\mathbf{K}^{uu}$ is the structural stiffness matrix, $\mathbf{K}_\sigma^{uu}$ is the geometric stiffness matrix, χ are the buckling eigenvalues and $\mathbf{u}_b$ is the buckling eigenvector, in order to determine the static thermal buckling temperatures for various modes (m, n) where m indicates the number of circumferential wave numbers and n indicates the axial mode number. The cylindrical shell is of mild steel material. The cylindrical shell has the following dimensions: 0.914 m long and 0.876 m radius. The thickness of the shell is 0.0015 m. The number of three node isoparametric line element used is 15. Table 1 lists the lowest buckling temperature (i.e., axial mode number $n = 1$) for various circumferential modes (m).

Table 1
Critical buckling temperature of the cylindrical shells with $l/r = 1.048$ for 25 modes

Modes	Buckling temperature (°C)
(1,1)	92.40
(2,1)	92.40
(3,1)	92.39
(4,1)	92.38
(5,1)	92.38
(6,1)	92.37
(7,1)	92.37
(8,1)	92.37
(9,1)	92.37
(10,1)	92.36
(11,1)	92.34
(12,1)	92.27
(13,1)	92.12
(14,1)	91.91
(15,1)	91.66
(16,1)	91.13
(17,1)	89.30
(18,1)	87.31
(19,1)	85.74
(20,1)	84.85
(21,1)	84.36
(22,1)	84.42
(23,1)	85.18
(24,1)	86.52
(25,1)	88.39

The buckling temperature presented in Table 1 are ΔT°C, where $\Delta T = (T_{actual} - T_o)$. Here T_o is the reference temperature (or stress free temperature) equal to 20°C, and T_{actual} represents the absolute buckling temperature. Table 1 gives an indication that the critical thermal buckling temperature does not vary to a great extent from mode to mode. The critical thermal buckling temperature being lowest for mode (21,1).

4.2. Critical mean axial velocity of fluid under steady flow condition

The critical velocity of water at various temperatures is required to be computed. Eq. (28) is used to compute the natural frequency of the cylindrical shell containing the flowing fluid at steady mean flow velocity, U_o. A LAPACK's eigenvalue solver RGG is used to solve Eq. (28). The temperature of water during the flow through shell is assumed to remain constant. Water at different temperature is considered in the study. Table 2 shows the critical velocity of water for various modes and various temperatures. Table 2 also lists the critical buckling temperature ($T_{actual}{}^{\circ}$C) for various modes.

As seen from Table 2, the critical flow velocity varies from mode to mode irrespective of the water temperature. Further the nature of variation of the critical flow velocity from mode to mode

Table 2
Critical velocity of water at specified temperatures and critical buckling temperature for the corresponding modes

Mode (m,n)	Critical velocity of water (m/s) at temperatures				Buckling temperature (T_{actual} °C)
	20°C	50°C	90°C	105°C	
(1,1)	164.0	147.5	104.0	57.0	112.4
(4,1)	161.5	146.5	103.0	57.0	112.38
(7,1)	125.5	121.5	104.0	57.0	112.37
(10,1)	99.5	91.0	77.5	55.5	112.36
(13,1)	98.0	84.0	61.0	49.0	112.12
(15,1)	101.0	83.5	53.0	34.5	111.66
(18,1)	112.5	91.0	48.5	5.5	107.31
(21,1)	129.5	104.5	52.5	0.0	104.36
(22,1)	136.0	110.0	56.5	0.0	104.42

at a particular temperature remains same. For example, considering water at temperature 20°C, the mode with lower harmonic has a high critical flow velocity. This velocity reduces as the number of harmonics increase, where it reaches a low for mode (13,1) which is about 98.0 m/s. Further the velocity increases as the number of harmonics increase. It should also be mentioned here that the mode (13,1) corresponds to the lowest natural frequency of the cylindrical shell. To illustrate further, consider the water flow through shell at temperature 90°C. It is again noted here that the mode (1,1) has the highest critical velocity. The velocity reduces as the number of harmonics increase, reaching a low value of 48.0 m/s for mode (18,1). For water flowing at temperature 105°C it is seen that the shell cannot sustain the flow of water at modes (21,1) and (22,1) since this temperature of water ($\Delta T = 85$°C) is very close to the critical thermal buckling temperature of the shell. Hence it is interesting to note that as the water temperature increases and is close to the thermal buckling temperature of the shell, the critical velocity of hot water will correspond to the mode(s) close to the thermal buckling temperature. That is (18,1) mode has buckling temperature of 87.3°C, hence the lowest velocity is 5.5 m/s with flow of water at 105°C. More detailed discussion on the above aspects can be found in article [20].

4.3. Computation of dynamic instability regions

The procedure involved in computing the regions of dynamic instability is as follows: (i) the structural stiffness, mass, geometric stiffness matrices, fluid–structure interaction matrix and kinetic energy of the fluid matrix are computed. (ii) These matrices are cast to form the equation of motion for a flow of fluid with harmonic perturbation, Eq. (30). (iii) This equation is required to be reduced to modal domain. Hence Eq. (30) is recast to Eq. (49) to obtain the undamped eigenvectors and added mass frequency of the cylindrical shell containing quiescent fluid. (iv) undamped eigenvectors are used to transform the equation of motion, Eq. (30), into the modal domain i.e., Eq. (50). (v) Eq. (50) is again cast in the state space form, Eq. (32). (vi) Floquet–Liapanov theorem is used to determine the stability information of the system. Fourth order Runge–Kutta method with Gill's coefficient is used to compute the transition matrix over one time period. For a given velocity and a range of frequency of pulsating fluid flow, the eigenvalues

of the transition matrix are examined. If the eigenvalues are less than one then the system is stable otherwise it will be unstable. The unstable points are plotted on a graph of 'pulsating frequency vs. steady velocity'.

The details of the finite element mesh comprise of 15 elements for the cylindrical shell and 30 elements for the fluid domain (two elements in the radial direction and 15 along the length of cylindrical shell). Cylindrical shell is of mild steel and water is considered as the working fluid. All material properties are independent of temperature.

4.3.1. Validation

The formulation for the study of the dynamic stability of cylindrical shells having the flow of pulsating fluid is validated with the theoretical results produced by Ginsberg [6], for a pipe of 4.57 m long, 0.1524 m in diameter and thickness of the pipe being 0.0013 m. The material was mild steel. Other details as mentioned in Ginsberg are: the component of harmonic flow velocity has a magnitude of 0.4 times the mean flow velocity. Damping is neglected. The ratio of mass of the fluid per unit length to the sum of mass of fluid per unit length of pipe and mass per unit length of pipe, α is 0.8. Typical result has been generated using the present computer code for a case of simply supported pipe for Ginsberg's dimensions. Water flow at ambient temperature (20°C) is considered.

Fig. 4 illustrate the comparison of the results reported by Ginsberg [6] and results obtained from the present methodology. The non-dimensional quantities are defined in Ginsberg [6]. The non-dimensional frequency is (Ω/ω_1), where Ω is the pulsating frequency of the fluid flow and ω_1 is the fundamental frequency of the fluid filled shell, given as $\pi^2\sqrt{EI/(\rho A+m)L^4}$, where E is Young's modulus of the pipe material, I the second moment of area of cross-section, ρ is the density of the fluid, A the internal cross-sectional area of pipe, m the mass per unit length of pipe and L the length of the pipe. The non-dimensional fluid velocity is defined as $(U_o/L\omega_1)$, where U_o is the component of steady flow velocity of the fluid. It is observed from the Fig. 4, that it is fairly

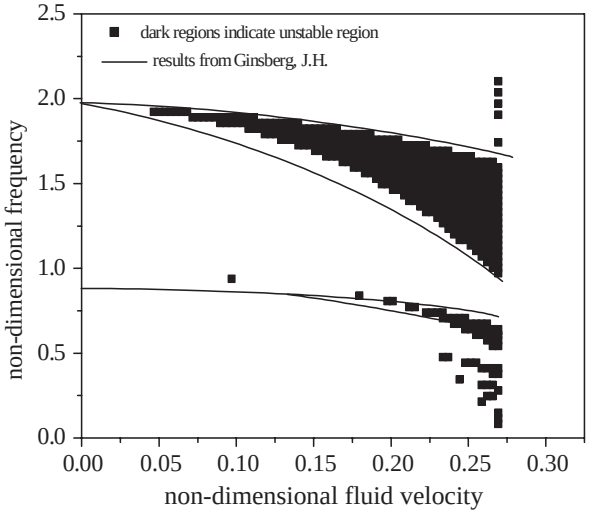

Fig. 4. Validation of present formulation with Ginsberg [6].

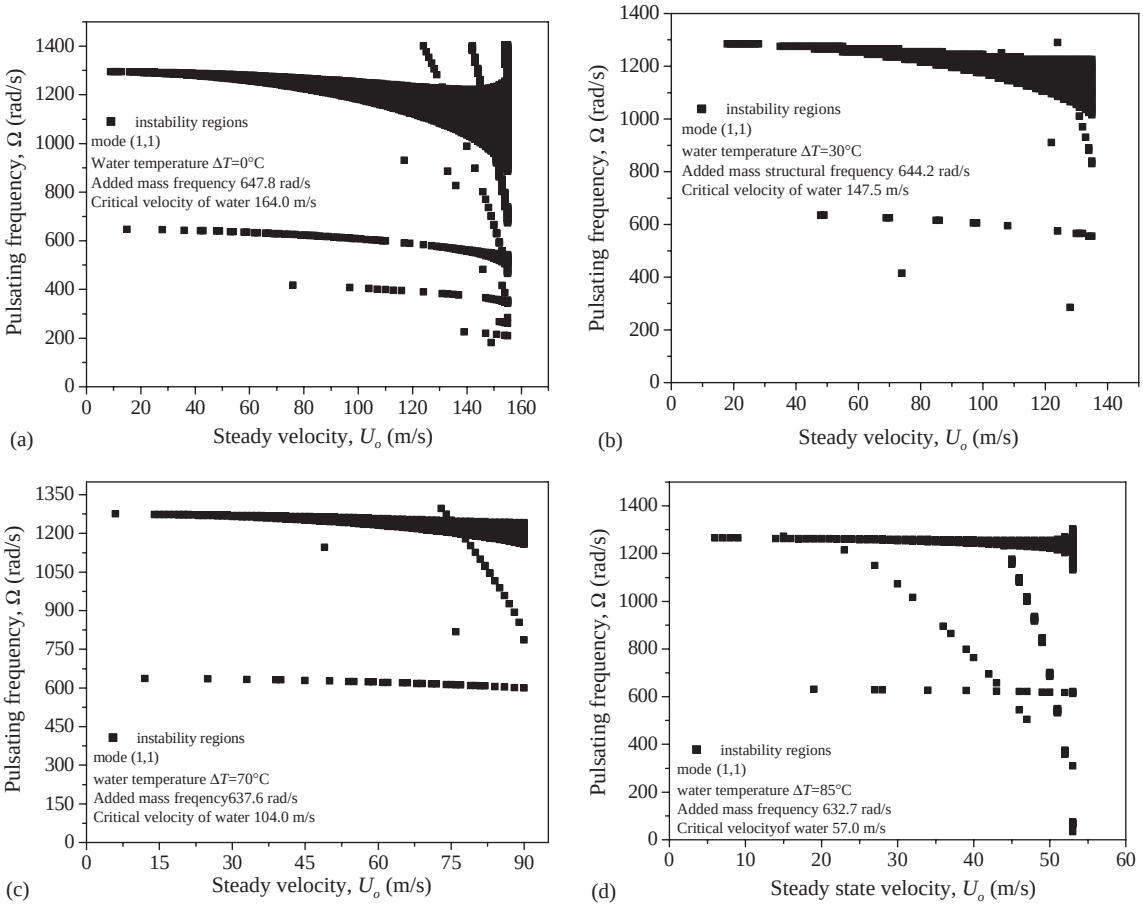

Fig. 5. Instability regions for mode (1,1). Excitation parameter, $\mu = 0.4$.

possible to evaluate the regions of instability by the present code and more or less the instability regions predicted by present study reasonably tally with that predicted by Ginsberg.

4.3.2. Stability studies on shells conveying hot fluid with fluctuating flow

To understand the nature of the occurrence of the regions of instability in cylindrical shells containing the flow with velocity varying harmonically, a detail study has been carried out on a typical cylindrical shell. The instability regions are evaluated for the cylindrical shell of dimension 0.914 m long and 0.876 m radius. The thickness of the shell is 0.0015 m. The magnitude of excitation parameter μ is taken as 0.4. Typical studies on the parametric instabilities are also presented with excitation parameter equal to 0.2 and 0.6. The ratio β_{MR} is 0.95, defined as $\beta_{MR} = (\rho_f A)/\rho_f A + m$, where ρ_f is the density of the fluid, A is the internal area of cross-section of shell and m is the mass per unit length of pipe. Water temperature considered in the study are 20°C, 50°C, 90°C and 105°C (or ΔT= 0°C, 30°C, 70°C and 85°C). The velocity of flow through the shell is limited by the critical velocity of the water at the stated temperature under steady flow condition, the details of which have been provided in Table 2. Hence in the present study

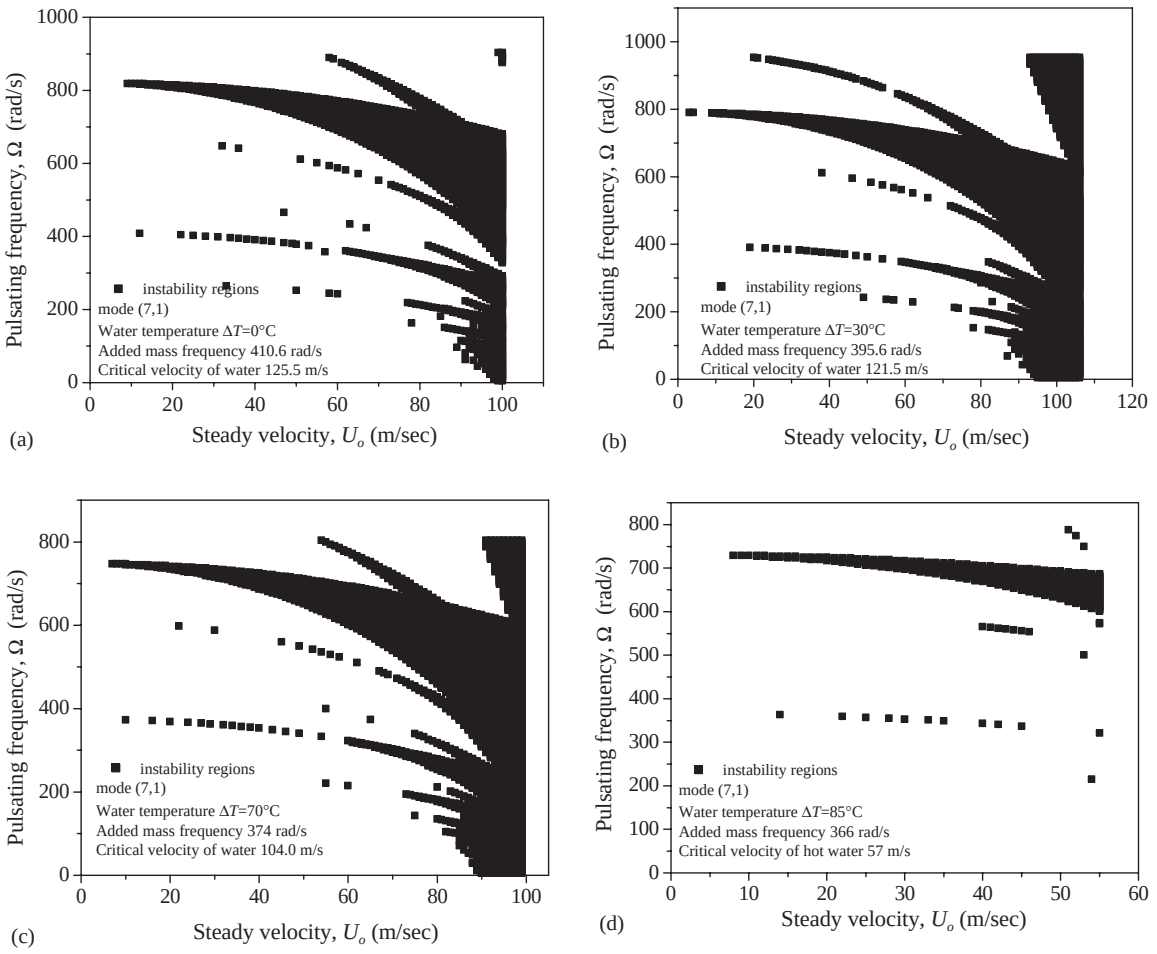

Fig. 6. Parametric resonance regions for mode (7,1). Excitation parameter, $\mu = 0.4$.

depending upon the circumferential mode and temperature of the water the evaluation of instability has been carried out up to critical flow velocity which corresponds to the case of uniform flow. The flow pulsating frequency is limited to more or less close to twice the natural frequency of the cylindrical shell containing quiescent fluid for the purpose of numerical evaluation. Studies are carried out for few modes like (1,1), (7,1), (13,1) and (18,1). Results of the numerical study are illustrated in Figs. 5–8, for excitation parameter, μ, equal to 0.40.

Consider the results of the study for mode (1,1). Referring to Fig. 5(a)–(d), we see that the resonance regions approximately happen to occur at $2\omega_{amf}$ and ω_{amf}. The instability region that originates close to $2\omega_{amf}$ appears to the dominant one as far the numerical results presented in this study. The interesting characteristics of this region are that the number of unstable points increases as the velocity increases and the unstable points appear for lower pulsating frequency, Ω, as the flow velocity increases. The width of the instability region widens as the flow velocity increases. This is true for flow of water at different temperatures of 20°C, 50°C, 90°C and 105°C.

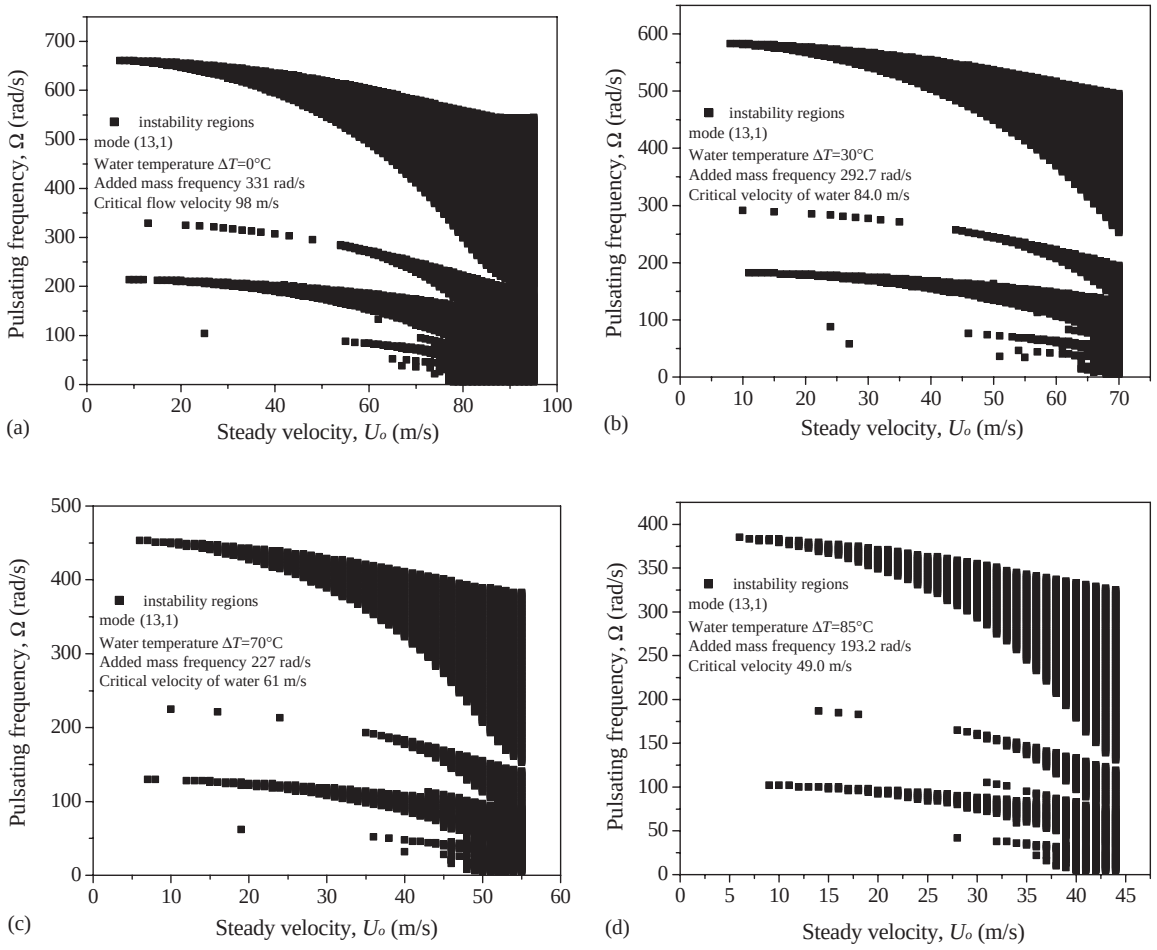

Fig. 7. Parametric resonance regions for mode (13,1). Excitation parameter, $\mu = 0.4$.

In the case of pipes containing the flow of fluid with flow velocity having a harmonic disturbance, it is known that the parametric resonance are generally found to appear in neighborhood of $(2\omega_{amf}/\bar{\bar{k}})$ where $\bar{\bar{k}} = 1, 2, 3, \ldots$ and ω_{amf} is the natural frequency of the system (strictly it is the frequency of the cylindrical shell containing the fluid) and also there is a specific range of, Ω, over which the resonance exists. The range of Ω depends on the excitation parameter, μ. When $\bar{\bar{k}} = 1, 3, 5$ the parametric resonance is primary resonance. The parametric resonance with $\bar{\bar{k}} = 1$, is of much importance. Secondary resonances appear for even values of $\bar{\bar{k}}$.

As the temperature of water increases, the critical flow velocity reduces, refer to Table 2. For example, in the case of mode (1,1), the critical flow velocity is 164.0 m/s for water at ambient temperature, 20°C and for water flowing at temperature of 105°C the critical flow velocity is 57.0 m/s. The thermal buckling temperature indirectly influences the magnitude of the critical flow velocity.

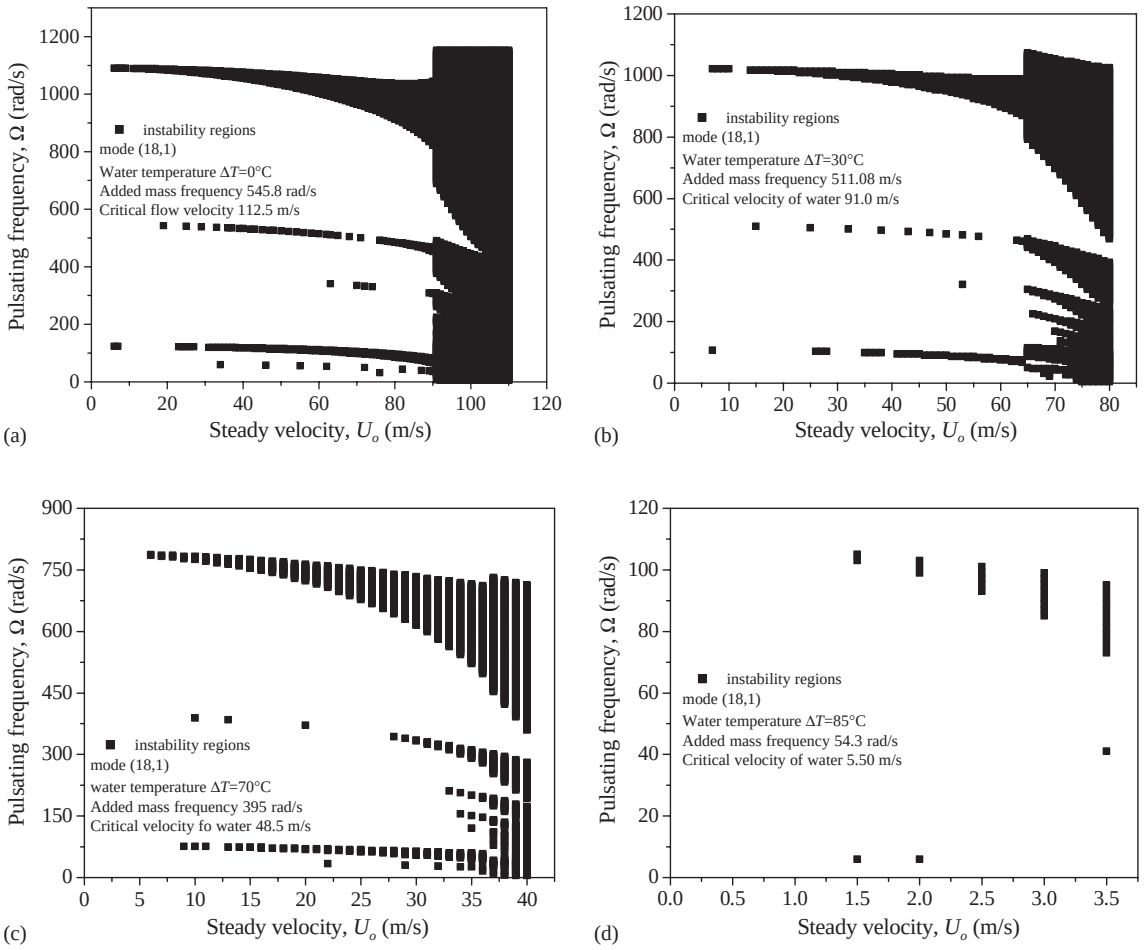

Fig. 8. Parametric resonance regions for mode (18,1). Excitation parameter, $\mu = 0.4$.

Apart from the resonance regions in and around $2\omega_{amf}$ there are instability regions around ω_{amf}. The resonance region around ω_{amf} is very small when compared to the one that occurs in and around $2\omega_{amf}$ which is the predominant parametric resonance.

Consider the instability regions for mode (7,1). Looking at the instability plots presented in Fig. 6(a)–(d), it is observed that the unstable points approximately start at $2\omega_{amf}$, and ω_{amf}.

The unstable points are very few in number that originate for pulsating frequency equal to ω_{amf} and also the number of unstable points increase for higher velocities. Also note the appearance of definite unstable points for higher flow velocities corresponding to pulsating frequencies which difficult to classify.

Under harmonically perturbed flow through cylindrical shells, it is observed that there exist only unstable regions for any value of pulsating frequency, Ω, of fluid flow very close to the critical flow velocity. For example, this can be observed in the case of mode (7,1), Fig. 6(a)–(c), for flow of water at 20°C, 50°C and 90°C. This typical characteristic feature occurs for velocity of fluid

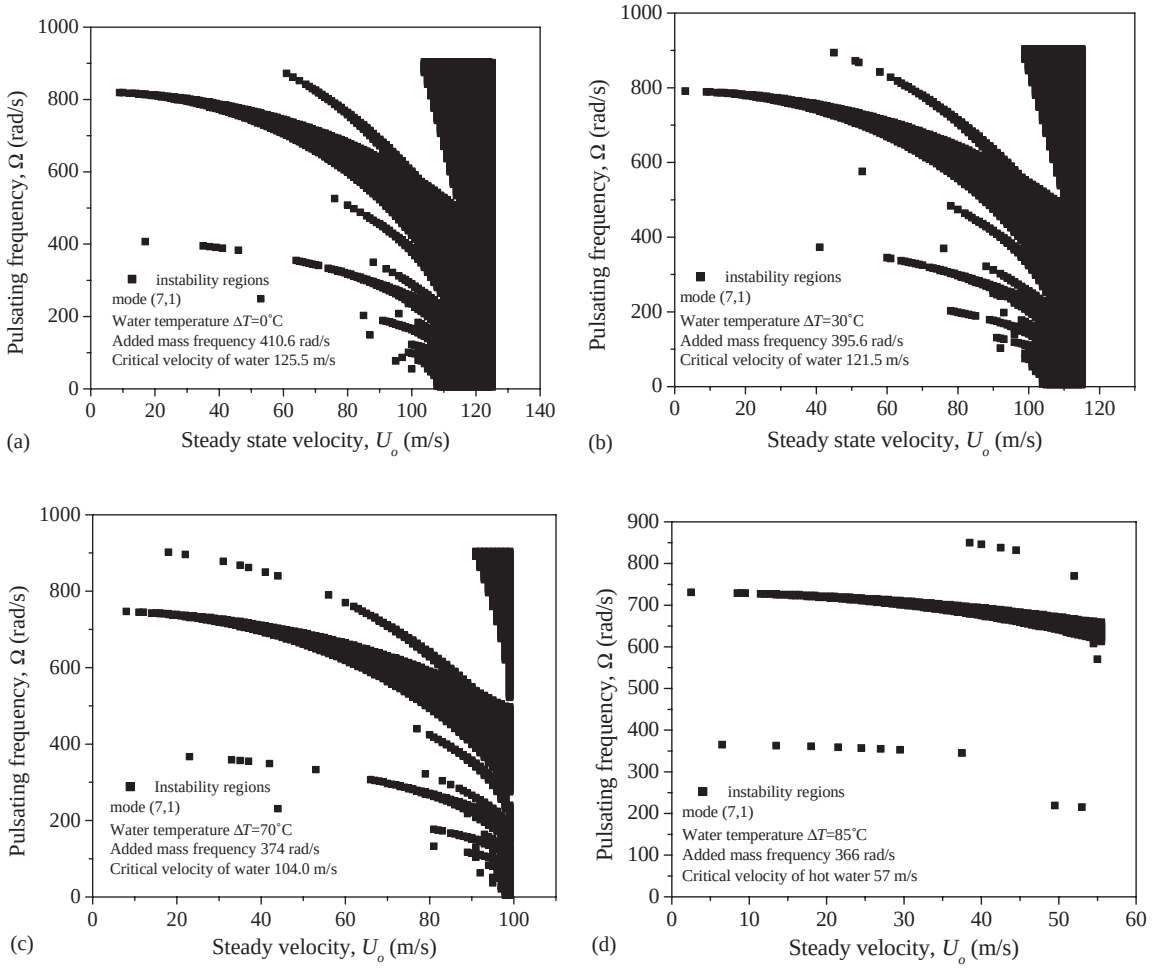

Fig. 9. Instability regions for mode (7,1). Excitation parameter, $\mu = 0.2$.

beyond 90%, 86% and 97% of the steady flow critical velocity where in the unstable region starts right from the smallest magnitude of the frequency of the pulsating fluid.

Fig. 7(a)–(d) likewise illustrates the instability regions for mode (13,1) due to flow of pulsatile cold water as well as hot water. For this mode we again notice that there exists another prominent instability region other than that originates at $2\omega_{amf}$ and ω_{amf}. Note the instability regions originating at 210 rad/s for water at ambient temperature, 198 rad/s for water at 50°C, 130 rad/s for water at 90°C and 100 rad/s for water at 105°C. For this mode (13,1) we also notice the presence of only unstable regions beyond certain percentage of the critical velocity. For example, for water temperature at 20°C and for velocity of water above 90% of the critical velocity and for water temperature of 90°C the velocity is 94% of the critical velocity, see Fig. 7(a) and (c).

Parametric resonance for mode (18,1) are presented in Figs. 8(a)–(d). The buckling temperature for this mode is 87.1°C. We have a case where water temperature of 85°C (or absolute temperature 105°C) is close to the buckling temperature of the shell. Under such conditions the

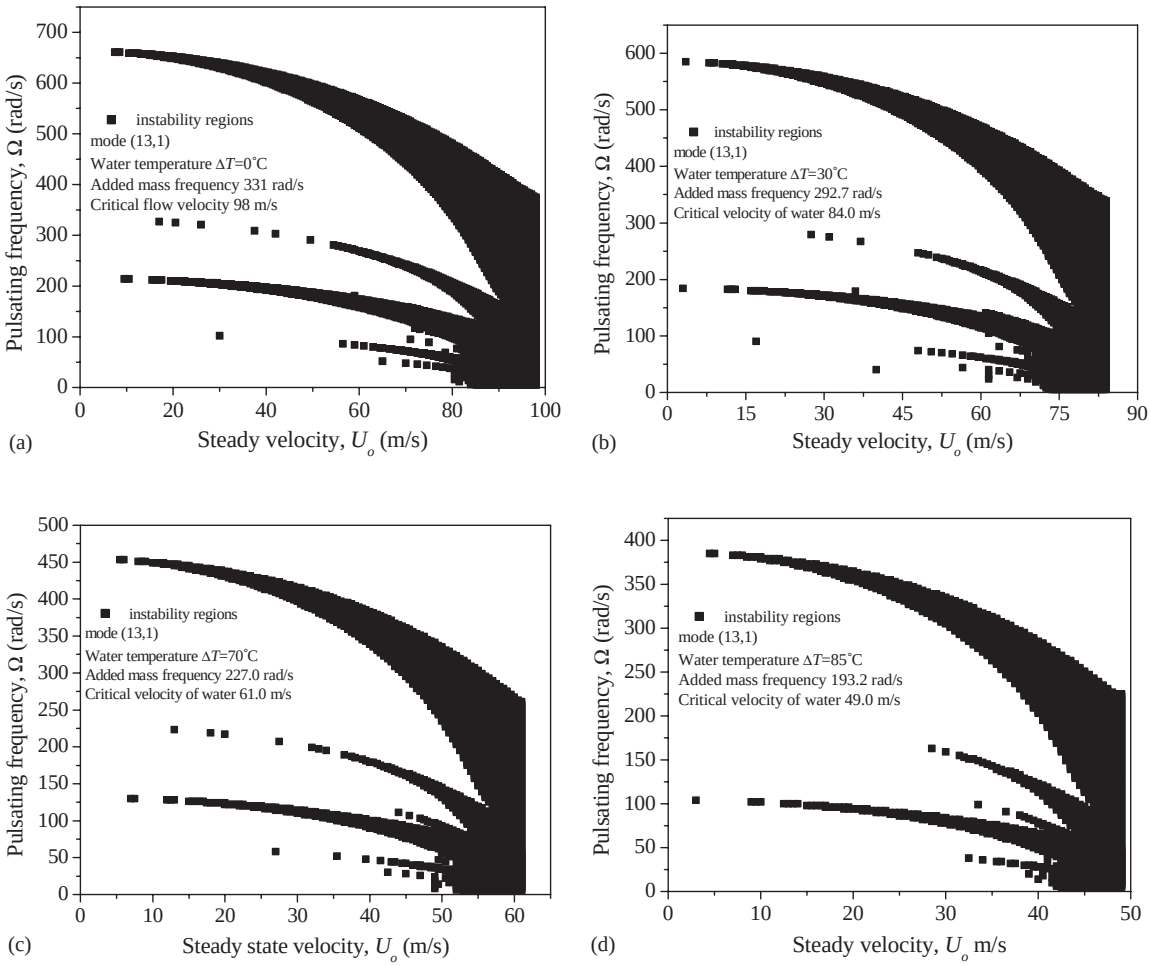

Fig. 10. Instability regions for mode (13,1). Excitation parameter, $\mu = 0.2$.

critical flow velocity of hot water under steady conditions will be very low equal to 5.5 m/s. The instability region observed for this mode have similar characteristics to that for modes (7,1) and (13,1).

It is also interesting to note that width of the instability regions observed for mode (1,1) are found to be very small compared to the width of the instability regions for modes (7,1) and (13,1).

4.4. *Effect of excitation parameter, μ, on the instability regions for pulsatile flow of hot water*

In order to study the effect of excitation parameter on the instability regions resulting from the pulsatile flow of water at various temperatures, typical results are presented in this section for mode (7,1) and (13,1). Excitation parameter equal to 0.2 and 0.6 are considered for the study. Figs. 9(a)–(d) and 10(a)–(d) illustrates the parametric instability regions for mode (7,1) and (13,1)

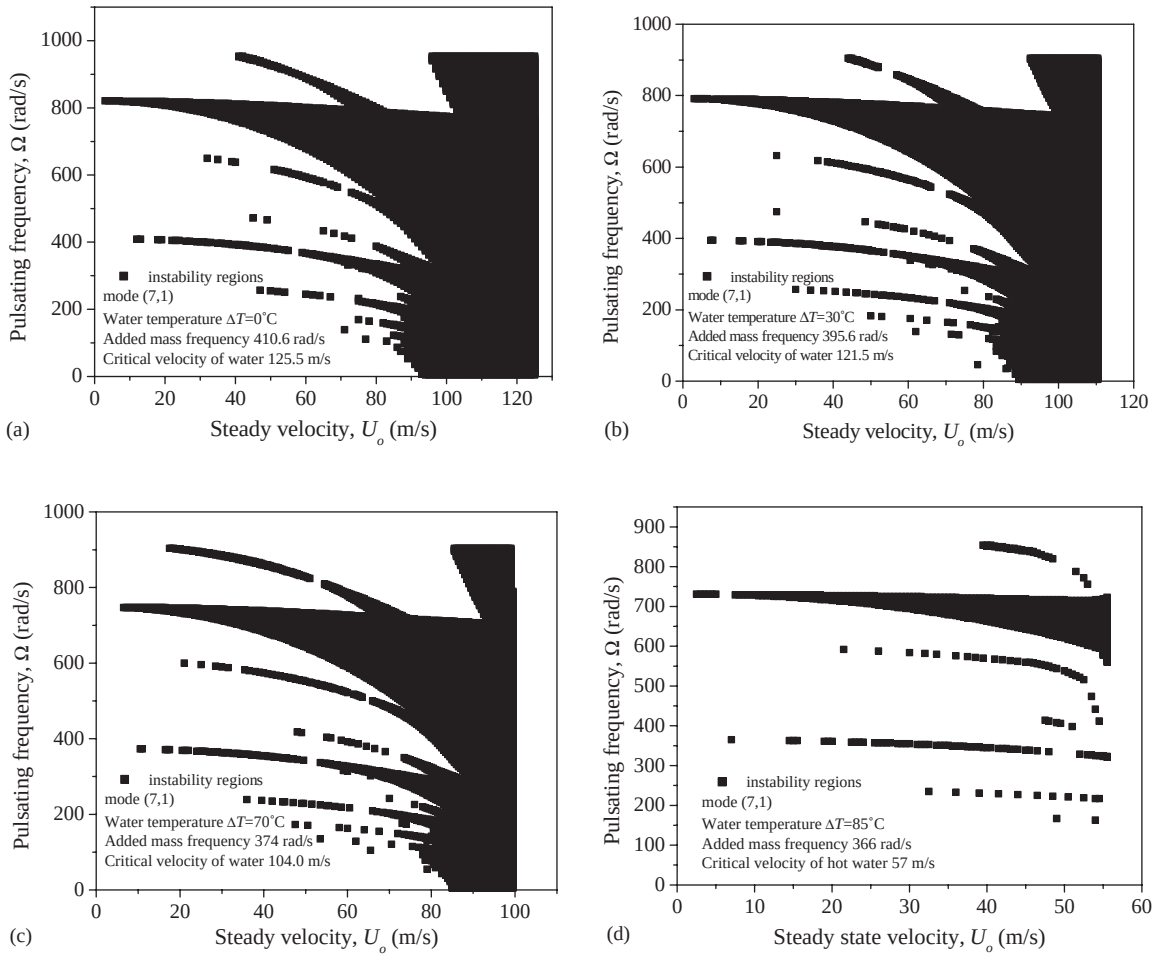

Fig. 11. Instability regions for mode (7,1). Excitation parameter, $\mu = 0.6$.

when the excitation parameter, μ, is equal to 0.20. When compared to instability regions obtained for $\mu = 0.4$, the instability regions have smaller width. Also notice that the instability regions droop down with greater gradient as the velocity increases. In other words the unstable points appear for lower pulsating frequency whereas the pulsating frequencies are higher in case of $\mu = 0.4$.

Typical results of the study for higher magnitude of excitation parameter $\mu = 0.6$ are also presented. Figs. 11 and 12 illustrate the instability regions for mode (7,1) and (13,1). It is clear on comparison of Fig. 11(a)–(d) with Fig. 6(a)–(d) or Fig. 9(a)–(d) that as the excitation parameter increases the width of the instability region also increases. It should also be noticed that the magnitude of the maximum steady state velocity beyond which there exists only unstable region decreases. For example, with pulsating flow having $\mu = 0.2$ and for mode (7,1) with water flow at ambient temperature, the maximum velocity is 88% of the critical velocity of water where as it is 75% of the critical velocity when excitation parameter is 0.6.

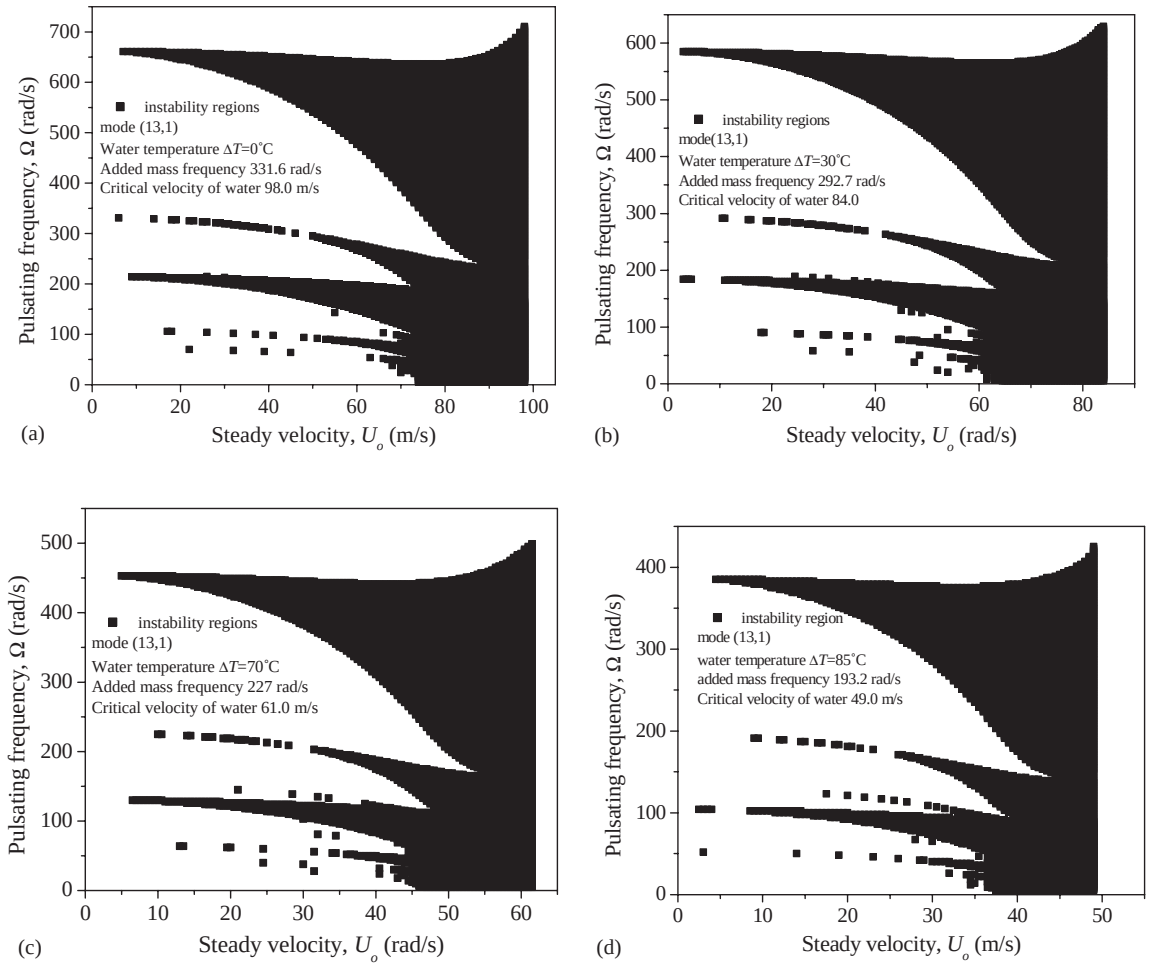

Fig. 12. Instability regions for mode (13,1). Excitation parameter, $\mu = 0.6$.

5. Conclusions

This paper attempts to study the parametric instabilities in cylindrical shells containing the flow of hot fluid which has harmonic disturbance. The temperature of hot water is considered to produce a uniform temperature rise across the thickness of the shell and due to perfect insulation the temperature gradient along the length of the shell will be negligible. These assumptions are favorable to understand the problem as the shell wall being subjected to thermal loading. By evaluating the geometric stiffness matrix due to initial stresses, it should help to understand this problem as an uncoupled thermomechanical problem due to the presence of hot fluid along with coupled fluid–structure interaction problem involving the flow of hot fluid through the cylindrical shell. Regions of parametric instabilities are evaluated for a typical cylindrical shell to illustrate the usefulness of the formulation. Higher circumferential

modes and its associated first axial mode have been considered in the evaluation. The conclusions from this study are:

(i) With the flow of hot fluid, water temperature greater than ambient, the regions of parametric resonance mostly originate for pulsating frequency of the fluid at $2\omega_{amf}$ and ω_{amf}. This finding is similar to that generally occurring in pipes/shells conveying pulsating fluid at atmospheric temperature. The resonance region which starts at $2\omega_{amf}$ has initially smaller width for lower steady velocity and gradually the width of the instability region increases as the flow velocity increases. The instability regions originating close to ω_{amf} are very small.
(ii) For certain higher modes like (13,1) and (18,1) the appearance of instability regions for pulsating frequency lower that ω_{amf} is observed. This instability region is comparatively wider compared to that originating for ω_{amf}.
(iii) For very high steady velocities (say for velocities beyond 85% of the critical velocity) there exist only unstable points.
(iv) Considering the influence of the excitation parameter on the instability regions, it is observed that lower the excitation parameter the width of the instability region reduces and the instability region droops with much larger gradient.

Acknowledgements

We express our thanks for a patient review of this article by the reviewers. Their comments were highly useful in improving the clarity of this article. Thanks are due to Dr. Padmanabhan Chandramouli (Assistant Professor, Machine Dynamics Laboratory, IIT Madras) for his contributions to this work during the revision of this article.

References

[1] D.S. Weaver, S. Ziada, M.K. Au-Yang, S.S. Chen, M.P. Paidoussis, M.J. Pettigrew, Flow-induced vibrations in power and process plant component-progress and prospects, *Transactions of the American Society of Mechanical Engineers, Journal, Pressure Vessel Technology* 122 (2000) 339–348.
[2] M.P. Paidoussis, N.T. Issid, Dynamic stability of pipes conveying fluid, *Journal of Sound and Vibration* 33 (3) (1974) 267–294.
[3] M.P. Paidoussis, C. Sundararajan, Parametric and combination resonances of a pipe conveying pulsating fluid, *Transactions of the American Society of Mechanical Engineers, Journal of Applied Mechanics* 42 (1975) 780–784.
[4] M.P. Paidoussis, N.T. Issid, Experiments on parametric resonance of pipes containing pulsatile flow, *Transactions of the American Society of Mechanical Engineers, Journal of Applied Mechanics* 43 (1976) 198–202.
[5] S.S. Chen, *Flow Induced Vibration of Circular Cylindrical Structures*, Hemisphere Publishing Co., New York, 1987.
[6] J.H. Ginsberg, The dynamic stability of pipe conveying a pulsatile flow, *International Journal of Engineering Science* 11 (1973) 1013–1024.
[7] S. Ariaratnam, N.S. Namachchivaya, Dynamic stability of pipes conveying pulsating fluid, *Journal of Sound and Vibration* 107 (1986) 215–230.
[8] M.P. Paidoussis, G.X. Li, Pipes conveying fluid: a model dynamic problem, *Journal of Fluids and Structures* 7 (1993) 137–204.
[9] M.P. Paidoussis, Flow-induced instabilities of cylindrical structures, *Applied Mechanics Review* 40 (2) (1987) 163–175.
[10] M.P. Bohn, G. Herrmann, The dynamic behavior of articulated pipes conveying fluid with periodic flow rates, *Transactions of the American Society of Mechanical Engineers, Journal of Applied Mechanics* 41 (1974) 55–62.

[11] U. Lee, C.H. Pak, S.C. Hong, The dynamics of a piping system with internal unsteady flow, *Journal of Sound and Vibration* 180 (2) (1995) 297–311.
[12] D.G. Gorman, J.M. Reese, Y.L. Zhang, Vibration of a flexible pipe conveying viscous pulsating fluid flow, *Journal of Sound and Vibration* 230 (2) (2000) 379–392.
[13] Y.L. Zhang, J.M. Reese, D.G. Gorman, Initially tensioned orthotropic cylindrical shells conveying fluid: a vibratory analysis, *Journal of Fluids and Structures* 16 (1) (2002) 53–70.
[14] Y.L. Zhang, J.M. Reese, D.G. Gorman, Finite element analysis of the vibratory characteristics of cylindrical shells conveying fluid, *Computer Methods in Applied Mechanics and Engineering* 191 (2002) 5207–5231.
[15] M. Amabili, F. Pellic, M.P. Paidoussis, Non-linear dynamics and stability of circular cylindrical shells containing flowing fluid. Part I: Stability, *Journal of Sound and Vibration* 225 (4) (1999) 655–699.
[16] M. Amabili, R. Garziera, Vibrations of circular cylindrical shells with nonuniform constraints, elastic bed and added mass. Part II: shells containing or immersed in axial flow, *Journal of Fluids and Structures* 16 (1) (2002) 31–51.
[17] J. Kochupillai, N. Ganesan, C. Padmanabhan, A semi-analytical coupled finite element formulation for shells conveying fluids, *Computers and Structures* 80 (3) (2002) 271–286.
[18] J. Kochupillai, N. Ganesan, C. Padmanabhan, A semi-analytical coupled finite element formulation for composite shells conveying fluids, *Journal of Sound and Vibration* 258 (2) (2002) 287–307.
[19] J. Kochupillai, N. Ganesan, C. Padmanabhan, Model reduction for parametric instability analysis in shells conveying fluid, *Journal of Sound and Vibration* 262 (2003) 633–649.
[20] R. Kadoli, N. Ganesan, Free vibrations and buckling analysis of composite cylindrical shell conveying hot fluid, *Composite Structures* 60 (1) (2003) 19–32.
[21] R. Ramasamy, N. Ganesan, Vibration and damping analysis of fluid filled orthotropic cylindrical shells with constrained viscoelastic damping, *Computers and Structures* 70 (1999) 363–376.
[22] P. Friedmann, C.E. Hammond, T.-H. Woo, Efficient numerical treatment of periodic systems with applications to stability problems, *International Journal for Numerical Methods in Engineering* 11 (1977) 1117–1136.
[23] S. Ramalingeswara Rao, N. Ganesan, Interlaminar stresses in shells of revolution, *Mechanics of Composite Materials and Structures* 3 (1996) 321–339.
[24] R.M. Jones, *Mechanics of Composite Materials*, Hemisphere Publishing Corporation, New York, 1998.
[25] C. Decolon, *Analysis of Composite Structures*, Hermes Penton Science, London, 2002.
[26] O.C. Zienkiewicz, R.L. Taylor, *The Finite Element Method, Solid and Fluid Mechanics, Dynamics and Non-linearity*, Vol.2, McGraw-Hill Book Company International Edition, New York, 1991.
[27] S. Ramalingeswara Rao, Static and Dynamic Problems in Laminated Beams and Axi-Symmetric Shells, PhD Thesis, Indian Institute of Technology Madras, India, 1997.
[28] R.D. Cook, D.S. Malkus, M.E. Plesha, *Concepts and Applications of Finite Element Analysis*, Wiley, Singapore, 2000.
[29] C.T.F. Ross, *Pressure Vessels under External Pressure: Statics and Dynamics*, Elsevier Applied Science, London, 1994.
[30] A.A. Lakis, P. Van Dyke, H. Ouriche, Dynamic analysis of anisotropic fluid-filled conical shells, *Journal of Fluids and Structures* 6 (1992) 135–162.
[31] G.H. Golub, C.F. Van Loan, Matrix Computations, Johns Hopkins Univ. Press, Baltimore, MD, 1996.